[Frontiers in Bioscience 5441-5461, May 1, 2008]

Structure and ligand interactions of the urokinase receptor (uPAR)

Magnus Kjaergaard[1,2], Line V. Hansen[1,3], Benedikte Jacobsen[1], Henrik Gardsvoll[1], Michael Ploug[1]

[1]Finsen Laboratory, Rigshospitalet section 3735, Copenhagen Biocenter room 3.3.31, Ole Maaloes Vej 5, DK-2200 Copenhagen N, Denmark, [2]SBiN-Lab, Department of Biology, University of Copenhagen, Copenhagen Biocenter room 3.0.41, Ole Maaloes Vej 5, DK-2200 Copenhagen N, Denmark, [3]DrugMode Aps, Forskerparken 10C, DK-5230 Odense M., Denmark

TABLE OF CONTENTS

1. ABSTRACT

The urokinase-type plasminogen activator receptor (uPAR or CD87) is a glycolipid-anchored membrane glycoprotein, which is responsible for focalizing plasminogen activation to the cell surface through its high-affinity binding to the serine protease uPA. This tight interaction (K_D less than 1 nM) is accomplished by an unusually large and hydrophobic binding cavity in uPAR that is created by a unique interdomain assembly involving all three homologous domains of the receptor. These domains belong to the Ly-6/uPAR (LU) protein domain family, which is defined by a consensus sequence predominantly based on disulfide connectivities, and they adopt a characteristic three-finger fold. Interestingly, the gene for uPAR is localized in a cluster of 6 homologous genes encoding proteins with multiple LU-domains. The structural biology of uPAR will be reviewed with special emphasis on its multidomain composition and the interaction with its natural protein ligands, *i.e*. the serine protease uPA and the matrix protein vitronectin.

2. INTRODUCTION

Localized activation of the abundant zymogen plasminogen, which is present at 2 micromolar in plasma, represents one of the important steps in vascular fibrinolysis as well as in proteolytic degradation of the extracellular matrix. Besides degrading fibrin and other matrix constituents such as fibronectin, vitronectin and laminin, the active, broadspectrum serine protease, plasmin, can also indirectly affect collagen turnover by activating certain matrix metalloproteases (MMPs). The combined activities of these proteases display an adequate proteolytic repertoire, enabling degradation of most protein constituents in the extracellular matrix barriers. Extracellular proteolysis is believed to be involved in several important physiological processes maintaining normal tissue homeostasis such as wound healing, involution of post-lactational breast tissue and bone morphogenesis, but also during pathological conditions such as cancer invasion and metastasis (1-3).

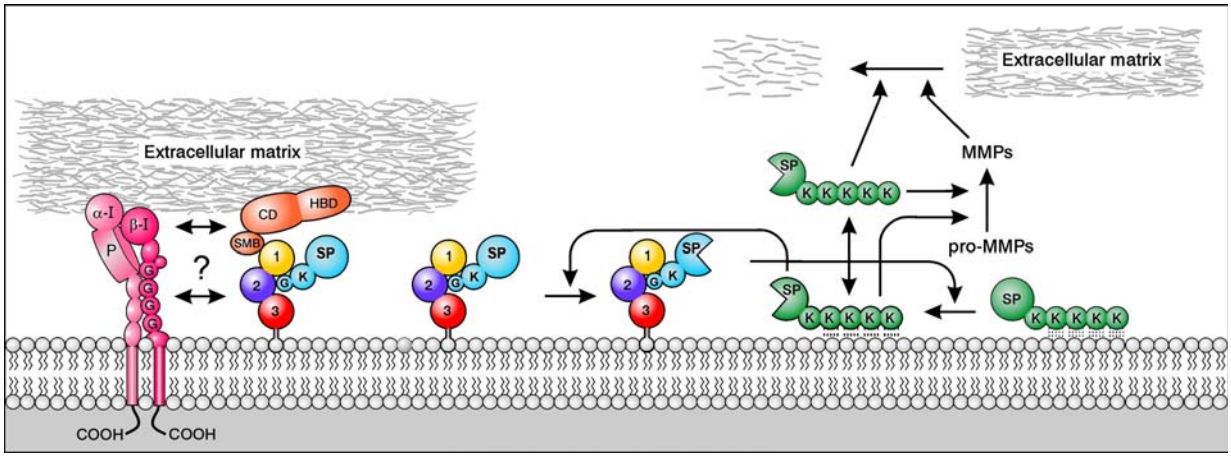

Figure 1. Cartoon of the involvement of uPAR in uPA-mediated plasminogen activation and in adhesion to the extracellular matrix. Membrane-tethered uPAR binds uPA (*light blue*) with high-affinity, thus restricting it to the vicinity of the cell membrane. Plasminogen (*green*) binds abundant, low-affinity lysine binding sites on the membrane. In this manner, the cell surface serves as a template to enhance the reciprocal zymogen activation of prouPA and plasminogen. Activation of plasminogen initiates degradation of the extracellular matrix directly or indirectly by activating certain pro-MMPs. uPAR also binds matrix-embedded vitronectin (*orange*), facilitating the subsequent matrix engagement of integrins (*pink*). These interactions allow cells to adhere to and migrate on vitronectin surfaces *in vitro*. Little is known about the interplay between uPAR and the integrins at the molecular level, and it is uncertain if the formation of a ternary complex between uPAR, integrin and vitronectin is required to elicit adhesion and migration on a vitronectin-containing extracellular matrix *in vivo*.

Activation of plasminogen is primarily mediated by two serine proteases with narrow substrate specificities, the urokinase-type plasminogen activator (uPA) and the tissue-type plasminogen activator (tPA), although other physiologically relevant plasminogen activators may exist (4). The efficiency of uPA-mediated plasminogen activation is greatly enhanced by the specific binding of uPA to its high-affinity receptor on the cell surface (5). Mechanistically, this urokinase-type plasminogen activator receptor (uPAR) is believed to enhance plasminogen activation by tethering prouPA to the membrane, where it encounters a local "high concentration" of membrane-associated plasminogen (Figure 1). Both plasmin and active two-chain uPA can mutually activate each others' inactive zymogen forms. This phenomenon is termed reciprocal zymogen activation and enables the positive feedback amplification that is inherent to the system - as illustrated in Figure 1. When the membrane acts as a template assembling these two zymogens, their low endogenous activity may be sufficient to initiate the activation of this cascade (6). Besides plasminogen, other proteases such as cathepsin B (7), matriptase (8, 9) and hepsin (10) are capable of activating prouPA *in vitro* and they may represent additional candidates for the initiation of the reciprocal zymogen activation. The activities of plasmin and two-chain uPA are both kept in check by their respective serpins, *alpha*$_2$-antiplasmin and plasminogen activator inhibitor-1, PAI-1.

Membrane associations of prouPA and plasminogen are thus important events in the regulation of plasminogen activation. First, as the activation of both proteases is facilitated by the abovementioned template effect, this system favours a focused generation of the proteolytic activity in the immediate vicinity of the cell surface. Second, this focalization is further augmented by the selectivity of the serpin *alpha*$_2$-antiplasmin. The efficient and fast inhibition of plasmin by *alpha*$_2$-antiplasmin requires access to both the active site of the protease domain and the low-affinity lysine binding sites present in the plasmin kringle domains. As the membrane association of plasmin actually occupies these low-affinity lysine binding sites, the surface-bound plasmin becomes refractory to the inhibitory effects of *alpha*$_2$-antiplasmin (11).

In addition to its primary involvement in the regulation of extracellular proteolysis, several other non-proteolytic functions have been reported for uPA and uPAR in cell adhesion and migration – for recent reviews see (12, 13). The main topic of the present review is focused on the protein structure of uPAR as well as various aspects of structure-function relationships in the interaction between uPAR and its *bona fide* ligands, uPA and vitronectin.

3. PRIMARY STRUCTURE OF uPAR

Until now, orthologous cDNA sequences encoding urokinase receptors from 10 different mammals have been published, 5 primates and 5 non-primates (14-19). These translate into 322-336 residues precursor proteins, which are further truncated into 274-283 residues long mature receptors after removal of N- and C-terminal signal sequences, which ensure proper secretion and glycolipid anchoring, respectively. Additional posttranslational modifications of uPAR include processing of 3-7 potential N-linked glycosylation sites, attachment of a C-terminal glycolipid-anchor and formation of 14 disulfide bonds. The fully processed uPAR is thus a

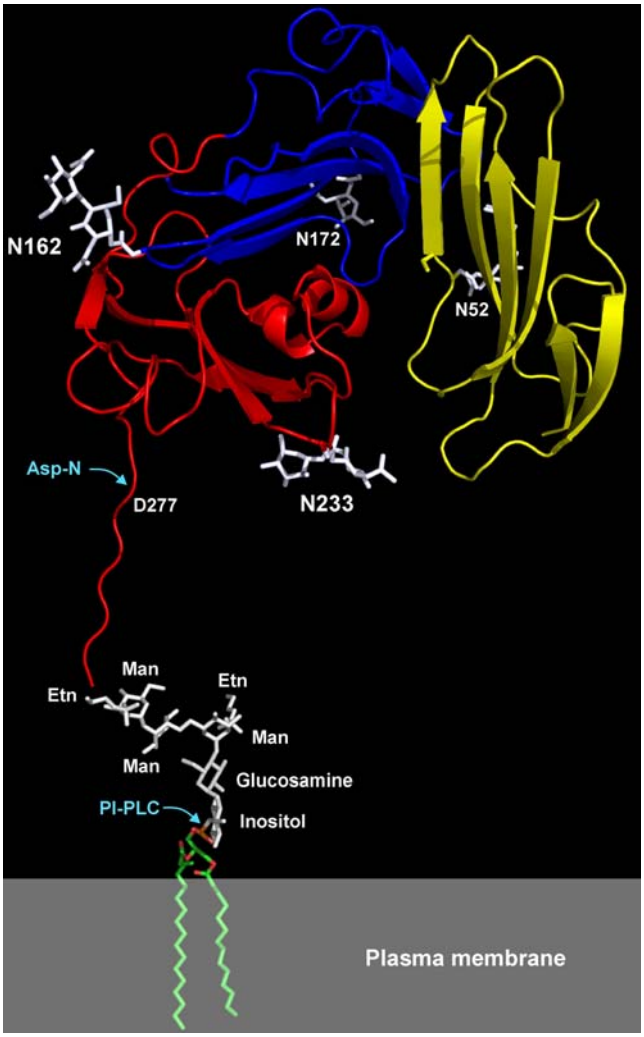

Figure 2. Schematic cartoon of the GPI-anchored uPAR. The carboxyl group of Gly^{283} in uPAR is via an amide bond covalently linked to a glycosylphosphatidylinositol moiety, which tethers uPAR to the outer leaflet of the cell membrane (20) The uPAR protein is shown as a ribbon diagram (DI *yellow*, DII *blue* and DIII *red*) with N-linked carbohydrates represented by the two innermost N-acetyl-glucosamine moieties and shown as white sticks. The minimal core unit of a GPI-anchor is shown to scale and its terminal ethanolamine (*Etn*) is joined to Gly^{283} of uPAR. The C-terminal linker region of uPAR (residues 275-283) is arbitrarily added as an extended strand in this cartoon as it is not defined by electron densities in any of the crystal structures solved (43-45). NMR and molecular dynamics studies of a GPI-anchor embedded in micelles demonstrate that the carbohydrate moiety is largely extended and capable of undergoing oscillatory motions (26), suggesting that the GPI-anchor forms a flexible linker allowing uPAR a considerable motional freedom relative to the membrane. Specific shedding of GPI-anchored uPAR from the cell surface can be accomplished by the action of specific phospholipases (*i.e. PI-PLC* and *PI-PLD*) or by specific proteases *e.g. Asp-N* (36) demonstrating the accessibility of this linker peptide.

cysteine-rich glycoprotein of moderate size, which contains no protein part exposed to the cytoplasm.

3.1. Membrane attachment of uPAR via a glycolipid-anchor

Examination of the cDNA-derived sequence for human uPAR revealed the presence of a stretch of moderately hydrophobic residues at the C-terminus. Originally, this was interpreted as the putative transmembrane segment accounting for the membrane attachment of uPAR (14). However, additional biochemical studies demonstrated that this peptide sequence actually serves as a signal sequence, targeting uPAR for posttranslational modification with a glycosylphosphatidylinositol (GPI) anchor. In this process, the moderately hydrophobic part of the C-terminus of uPAR is removed (20), and the newly formed C-terminus is linked to a preformed GPI-anchor, thereby tethering uPAR directly to the outer leaflet of the lipid bilayer (20) – as shown schematically in Figure 2. The exact attachment site of the GPI-anchor was revealed by amino acid composition analysis of the

purified protein isolated from U937 cells (20) and later confirmed by site-directed mutagenesis (21). Although Gly^{283} was identified as the most probable attachment site in uPAR, it was nevertheless demonstrated that neighbouring residues could be exploited as attachment sites as well (21). In human uPAR, both Ser^{282} and Gly^{283} comply with the consensus sequence established for GPI-attachment (22, 23), which provides an explanation for the promiscuity observed by site-directed mutagenesis for the actual GPI-anchoring site in human uPAR (21).

Membrane anchoring via glycolipids has a number of functional and structural implications for this group of membrane proteins as compared to the traditional attachment via transmembrane *alpha*-helices or *beta*-barrels. A study based on fluorescence resonance energy transfer between a GPI-anchored protein and a reconstituted membrane showed that the GPI-anchor allows the protein to come into close contact with the membrane (24). Accordingly, studies by nuclear magnetic resonance on the structure and dynamics of the glycan moiety of the GPI-anchor, both as a free entity and embedded into lipid micelles, reveal the GPI-anchor to be largely extended and undergoing oscillatory movements relative to the membrane (25, 26). The general picture emerging from these studies is that the GPI-anchor provides a flexible linker endowing the attached protein with a considerable amount of spatial freedom relative to the membrane. This flexibility could be functionally important for uPAR as it would enable the receptor to adopt favourable orientations relative to its interaction with uPA and its matrix-embedded ligand, vitronectin.

The GPI-anchorage also has several important functional implications for uPAR that are directly related to the dynamic partitioning and lateral mobility of uPAR in the plasma membrane. First, since uPAR is devoid of a cytoplasmic domain, and as a consequence does not penetrate the plasma membrane, it is *a priori* unable to elicit transmembrane signalling without recruitment of other proteins. Some insights into a possible mechanism behind signalling by GPI-anchored proteins in general have recently emerged from studies by single-molecule tracking of the GPI-anchored CD59, which showed that ligand-induced clustering caused a transient confinement of CD59 into a relative immobile membrane microenvironment (27). Importantly, this temporal arrest in lateral mobility of the CD59 clusters coincided with the recruitment of signalling molecules from the *Src*-kinase family and their intracellular interaction partners. These membrane confinements showed a strict requirement for the glycolipid-anchoring of CD59 (27). Second, the lack of a transmembrane segment confers GPI-anchored proteins with a higher lateral mobility in the absence of interactions with extracellular proteins (28). In line with this observation, it was proposed that the ligand-free uPAR possessed a high lateral mobility, which could be reduced by uPA binding (29). Third, a very important consequence of being GPI-anchored relates to the differential partitioning of these membrane proteins into specialized microdomains of the cell membrane. Generally, GPI-linked proteins seem to be predominantly sequestered in certain detergent-resistant and cholesterol/sphingolipid-enriched microcompartments of the membrane known as lipid rafts (30). This distribution was also found to hold true for uPAR (31, 32). One important functional implication of this unique membrane compartmentalization of uPAR is related to the availability and local abundance of potential interaction partners. In compliance with this consideration, it was demonstrated that the glycolipid-anchored uPAR preferentially interacts with soluble vitronectin if uPAR is sequestered in lipid rafts, as judged by immunoprecipitation experiments (33). The elevated local concentration of uPAR arising as a consequence of such selective partitioning and sequestering in the relative immobile environment of lipid rafts may thus provide uPAR molecules with an apparent "functional multivalency". Similarly, the prevalence of uPA-mediated cleavage of uPAR is also higher if the uPA-uPAR complexes cluster in lipid rafts (33).

3.1.1. Paroxysmal nocturnal hemoglobinuria

A unique consequence of being GPI-anchored in a pathological perspective is the deficient expression of uPAR on the cell surfaces of peripheral blood cells that are derived from bone marrow stem cells affected by the haematological disorder paroxysmal nocturnal haemoglobinuria, PNH (34). The common genetic defects causing this disease are acquired somatic mutations affecting the X-linked PIG-A gene, which encodes a subunit of the N-acetyl-glucosamine phosphatidylinositol transferase involved in the first step in the biosynthesis of GPI-anchors (35). Consequently, leukocytes affected by PNH secrete a soluble form of uPAR lacking the entire GPI-anchor and the C-terminal signal sequence, but maintaining its high affinity for uPA binding (36).

3.2. Glycosylation pattern of human uPAR

When analyzed by SDS-PAGE under reducing conditions, human uPAR appears as a single, broad band with a mobility corresponding to a molecular weight of 50-60 kDa, which can be reduced to approximately 35 kDa by N-glycanase treatment (37-39). This demonstrates that human uPAR is comprised of a single polypeptide chain containing a high level of heterogeneous N-linked glycosylation. Accordingly, sequence analysis reveals that human uPAR contains 5 potential N-linked glycosylation sites located on Asn^{52}, Asn^{162}, Asn^{172}, Asn^{200} and Asn^{233}. Studies on recombinant soluble uPAR expressed by Chinese hamster ovary (CHO) cells demonstrate that carbohydrate can in fact only be recovered on the first four glycosylation sites (40). The impaired glycosylation of Asn^{233} is probably related to its position close to the C-terminus, which in model systems is sufficient to abrogate glycosylation (41). A recombinant form of uPAR harbouring only short biantennary carbohydrates can be produced in S2 cells from *Drosophila melanogaster (*42). The uPA binding kinetics of this recombinant form is comparable to that of uPAR expressed in CHO cells, as determined by surface plasmon resonance (42). The homogeneous glycosylation of S2 cell-produced uPAR is highly advantageous for structural studies, as sample heterogeneity generally impedes crystallization. Thus, all crystal structures solved so far for human uPAR have used recombinant protein produced by S2 cells (43-45), and in

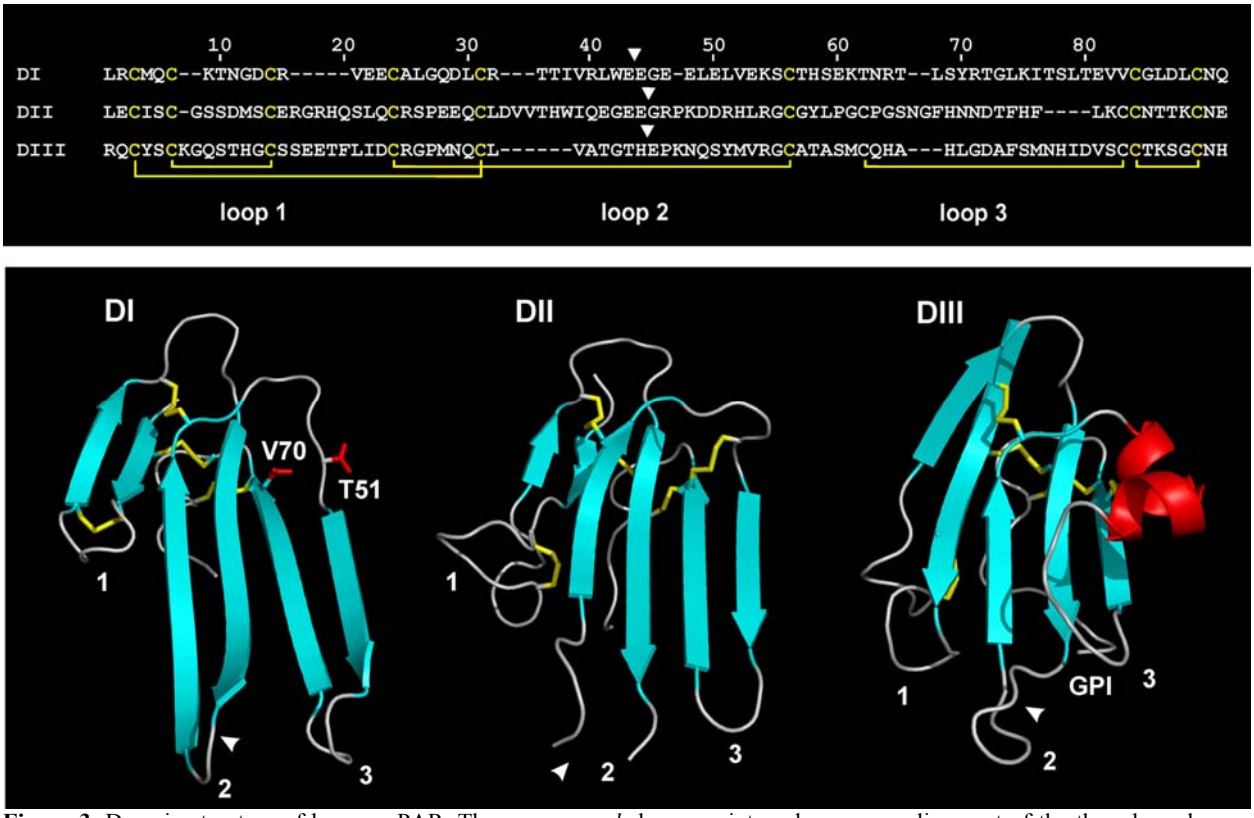

Figure 3. Domain structure of human uPAR. The *upper panel* shows an internal sequence alignment of the three homologous domains in human uPAR using Clustal W. Interdomain linker regions are omitted for clarity, and the DI is represented by residues 1-78, DII by residues 93-178 and DIII by residues 192-273. Positions of introns in the uPAR gene (PLAUR) dividing the coding regions for the individual domains into separate exon sets are shown as arrowheads. The experimentally assigned disulfide connectivity is shown by yellow lines (43, 49). In the *lower panel*, the individual domains of uPAR are shown as cartoon representations using the structure of uPAR solved in complex with a peptide antagonist by X-ray crystallography (pdb: 1YWH). The following colour coding is used: *beta*-sheets (*cyan*), *alpha*-helices (*red*) and disulfide bonds (*yellow*). The location of the C-terminal GPI-attachment is indicated and the positions equivalent to the lacking consensus disulfide bond in uPAR DI are specified (Thr^{51} and Val^{70}).

two cases, selected glycosylation sites have even been silenced by site-directed mutagenesis (43, 45). Removal of the carbohydrate at Asn^{52} either by site-directed mutagenesis or by enzymatic deglycosylation causes a moderate effect on the affinity of uPAR towards uPA (40, 42, 46, 47). Accordingly, the accessibility of the carbohydrate moiety on Asn^{52} for enzymatic deglycosylation is reduced when uPAR is bound to uPA (40). All other glycosylation sites can be removed without affecting the affinity towards uPA (42). Nonetheless, a combined removal of all glycosylation sites in human uPAR severely compromises the expression yields, possibly related to a reduced solubility of the product (42).

4. TERTIARY STRUCTURE OF uPAR

4.1. Domain structure

Shortly after the sequencing of its isolated cDNA, it was noticed that uPAR was devoid of an intracellular protein part and that the extracellular part was comprised of 3 repeats of a single, approximately 90 residues long, sequence motif (20, 48). The overall sequence identity between these repeated elements is relatively modest (14 to 28% sequence identity). Nevertheless, the nature of the repeated motif prompted the proposal that uPAR consists of 3 homologous domains separated by two approximately 15 residues long linker regions. The consensus sequence defined by these repeated motifs is primarily based on a conserved pattern of cysteines and a C-terminal invariant asparagine; see sequence alignment in Figure 3, upper panel. Importantly, the experimental assignment of the cysteine connectivity in the first of these putative uPAR domains revealed that the established disulfide bonds were all contained within this domain I (residues 1-87) and that this domain concordantly can be released from the rest of the molecule by limited proteolysis under non-denaturing and non-reducing conditions (49). The linker region connecting uPAR domains I and II is highly susceptible to cleavage in vitro by chymotrypsin (48) as well as by a number of physiologically relevant proteases in v*itro* or *in vivo* such as uPA (50-52), MMP-12 (53), the type-II transmembrane human airway trypsin-like protease (54), tissue kallikrein 4 (55), neutrophil elastase and cathepsin G (56). The remarkable susceptibility of this region to

cleavage by almost any protease with trypsin-like specificity suggests that the linker is fully accessible, and presumably unstructured, as would be expected for a true interdomain linker region. Nonetheless, it is noteworthy that uPA, the natural high-affinity protease ligand for uPAR, also cleaves this linker region despite the fact that this protease has a very restricted substrate specificity, and only few known physiological substrates have been identified. In agreement, the linker between uPAR domains I and II does indeed contain a uPA cleavage site (NSG**R**^{83}AV) that is almost identical to the preferred P3-P2' subsite specificity of uPA (SG**R**SA) as determined experimentally (57). Cleavage of uPAR in this linker region severely compromises both uPA binding (58) and vitronectin binding (51, 59), thus demonstrating that maintenance of the multidomain receptor status is required for both these interactions. The proteolytic cleavage of uPAR could therefore provide a possible regulatory mechanism to attenuate cell surface-associated plasminogen activation. Although this cleavage as mentioned above abrogates the uPAR-uPA and uPAR-vitronectin interactions, it has been hypothesized that the cleaved receptor might obtain new functionalities. Multiple studies have thus reported that the remaining uPAR domains II+III fragment contains a chemotactic neoepitope, which allegedly assigns a function to this fragment in cell migration and stem cell mobilization (60-62). This interesting topic is, however, considered outside the scope of this review, and the reader is therefore referred to recent comprehensive reviews for further information (13, 63).

4.1.1. LU-domain fold

Database searches revealed that uPAR is homologous to the GPI-anchored single domain proteins of the Ly-6 antigen family and the secreted elapid snake venom *alpha*-neurotoxins (64). This protein domain family was subsequently named the Ly-6/uPAR (LU) family[I]. Members of this family comprise both secreted, GPI-anchored as well as transmembrane type-I proteins (65). The three-dimensional structures have been solved for several of the single domain members, and they all confirmed the existence of a conserved fold for the LU-domains. This structure, known as the three-finger fold, is dominated by three loops forming a large 5 to 6-stranded anti-parallel *beta*-sheet (Figure 4). A nomenclature for the secondary structure elements has been assigned for the three-finger fold, where the *beta*-strands are named sequentially *beta*A, *beta*B etc. (66), and this nomenclature has been further expanded to cover proteins containing multiple LU-domains, by including the individual domain number from the N-terminus, *e.g. beta*IA, *beta*IB *etc*. (43). All four conserved disulfide bonds are found in the globular base of the LU-domains from which the fingers (*i.e.* loops) protrude. While the globular core and the *beta*-strands generally are preserved amongst the family members, more variability is allowed at the tip of the protruding loops. This translates into considerable heterogeneity in loop length, structure and ability to accommodate non-consensus disulfide bonds, as exemplified by the additional extra pair of cysteines present in loop 1 of all uPAR domains (Figure 3) and in loop 2 of certain long snake venom *alpha*-neurotoxins such as *alpha*- and *kappa*-bungarotoxin (Figure 4, *upper panel*). Introns in genes are often found in regions encoding surface-exposed and variable loop structures (67), and in the case of uPAR, these positions are accordingly localized at the tips of loop 2 in all of its three LU-domains (Figure 3). The third loop of the three-finger fold also appears quite versatile as it may adopt a *beta*-hairpin formed by *beta*E and *beta*F, which is required for the multidomain assembly of uPAR (*i.e.* DI and DII - Figure 3) and for the homodimerization of *kappa*-bungarotoxin (68), a mixed secondary structure comprising either *alpha*E and *beta*F (*e.g.* uPAR DIII and CD59), or a random coil-E and *beta*F as observed in the majority of snake venom *alpha*-neurotoxins (Figure 4).

The identification of the LU-domains in uPAR was originally based on a conserved set of 5 disulfide bonds and a single conserved asparagine (48). It was, however, recognized that the majority of snake venom *alpha*-neurotoxins only contained 8 cysteines, which led to a revision of the consensus cysteine spacing for the prototype LU-domains (65). The non-consensus disulfide bond that has been found in many mammalian LU-domains is linking the *beta*-strands *beta*A and *beta*B in loop 1, and is present in all three uPAR domains (Figure 3), CD59 (69) and in a few weak *alpha*-neurotoxins such as bucandin and denmotoxin A (70, 71). For CD59, this disulfide bond could be deleted by site-directed mutagenesis without affecting the expression or function of the protein (72), and the corresponding disulfide bond in uPAR DI can also be removed without affecting uPA binding (our unpublished results). These observations therefore suggest that this particular non-conserved disulfide bond may not be strictly required for proper folding of the LU-domain. Many long chain *alpha*-neurotoxins contain an additional disulfide in the second loop, *e.g. alpha*- and *kappa*-bungarotoxins (Figure 4, *upper panel*). This additional bond was found to be important for the specific function, but not for the overall structure of these toxins (73, 74), suggesting that this particular disulfide bond represents a functional adaptation rather than a structural requirement for the stability of the domain fold.

4.2. The uPAR-like gene cluster

Examination of the gene structures of human and mouse uPAR reveals that each of the three homologous uPAR domains are encoded by a separate exon set flanked by phase-1 introns, suggesting that the multidomain structure of uPAR arose by duplication of an ancestral single domain gene (49, 65, 75, 76). Further data-mining of open reading frames within 2 Mb of the PLAUR gene encoding human uPAR on the human chromosome 19q13 identified several GPI-linked proteins containing at least 2 LU modules (Figure 5). This new gene cluster contains all hitherto recognized multidomain members of the LU-protein domain family (*i.e.* uPAR, C4.4A, PRV-1 and TEX101) as well as two new candidate proteins (PRO4356 and GPQH2552). A few proteins having a two-domain LU-signature have been identified in other species, *e.g.* the GPI-anchored Robo-1 in rats (77) and the secreted *gamma*-inhibitors of phospholipase A_2 found in snake plasma (78, 79), but none of these have a human ortholog in the present uPAR-like gene cluster.

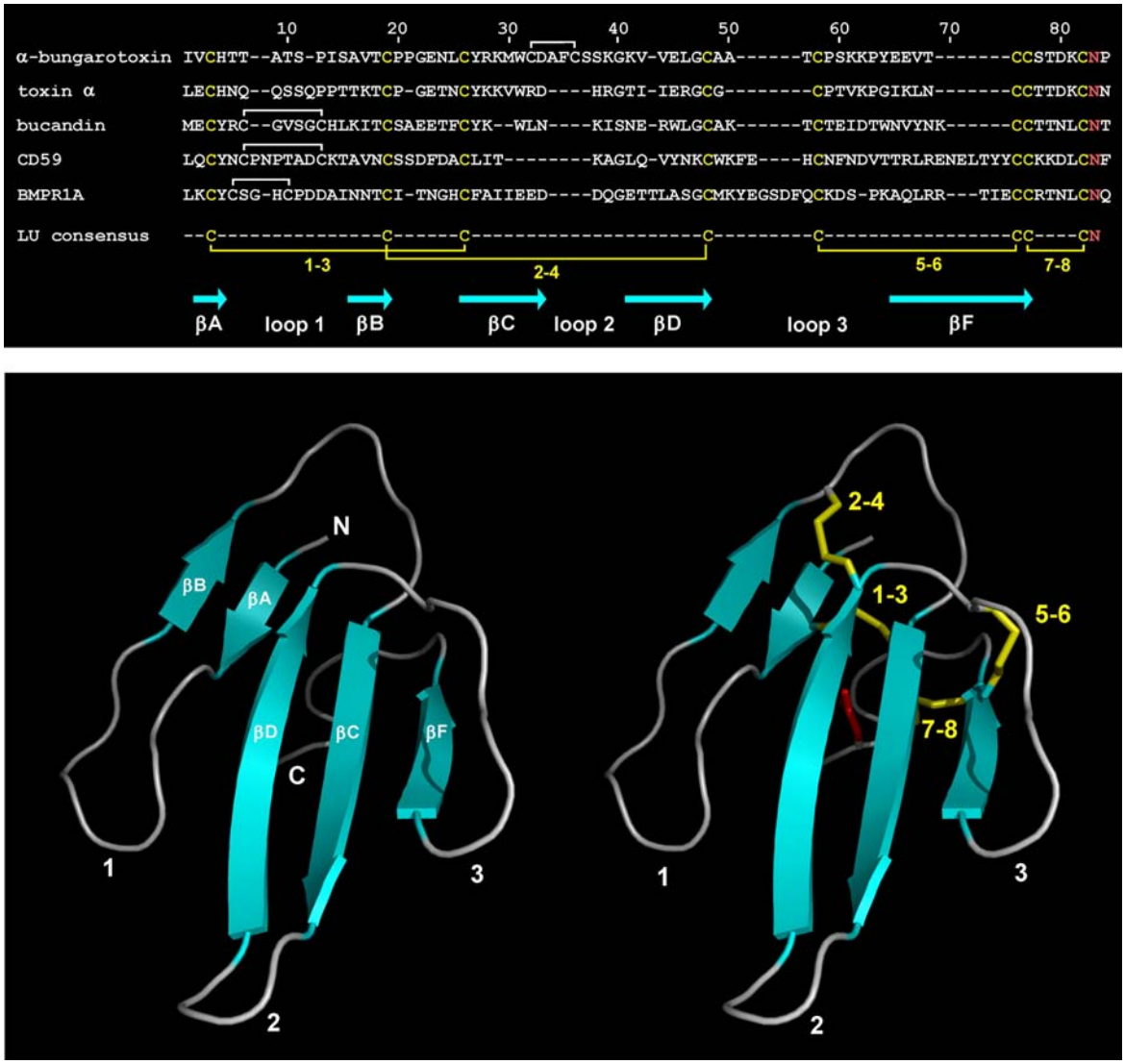

Figure 4. Consensus sequence and three-finger fold for LU-domains. Sequence alignments for a few representative members of the Ly-6/uPAR family are shown in the *upper panel*. These include secreted snake venom *alpha*-neurotoxins (*alpha*-bungarotoxin, toxin *alpha* and bucandin), the GPI-anchored complement regulatory protein CD59 and the extracellular ligand-binding domain of bone morphogenetic protein receptor type-1A (BMPRIA) belonging to the membrane type-1 TGF-*beta* receptor family. The four consensus disulfide bonds (*yellow*) and the invariant asparagines (*red*) defining the LU-domains are highlighted along with secondary structure elements. Individual non-conserved disulfide bonds are shown in white. The prototype three-finger fold for the LU-domains is shown in the *lower panel* as typified by the ribbon diagram representations for toxin *alpha* using the 1NEA coordinates. Consensus disulfide bonds are shown as yellow sticks, the conserved asparagine at the C-terminus is shown as a red stick and the *beta*-sheet nomenclature is indicated.

Unfortunately, none of the multidomain proteins we have identified so far in this uPAR-like gene cluster are as well characterized as uPAR from a structural point of view. C4.4A was originally identified as an antigen being upregulated *in vitro* in metastasizing pancreatic tumour cell lines (80). The association of C4.4A to progression of human cancer is illustrated by its expression in skin melanomas (81), esophagus cancer (82), and in particular by its strong correlation to poor survival in pulmonary non-small cell adenocarcinomas (83). Although the biochemical function of C4.4A is yet unknown, it is not an alternative receptor for uPA (84). No function has as yet been ascribed to the other multidomain members, but PRV-1 (CD177) is a biomarker for the benign haematological disease polycythemia rubra vera (85), and TEX101 has been found to be expressed in germ cells in murine gonads (86).

Intriguingly, the N-terminal LU-domains of all these multidomain proteins represent a notable exception to the conserved disulfide pattern in the LU-domain fold, as they all lack the disulfide between cysteines 5 and 6, which

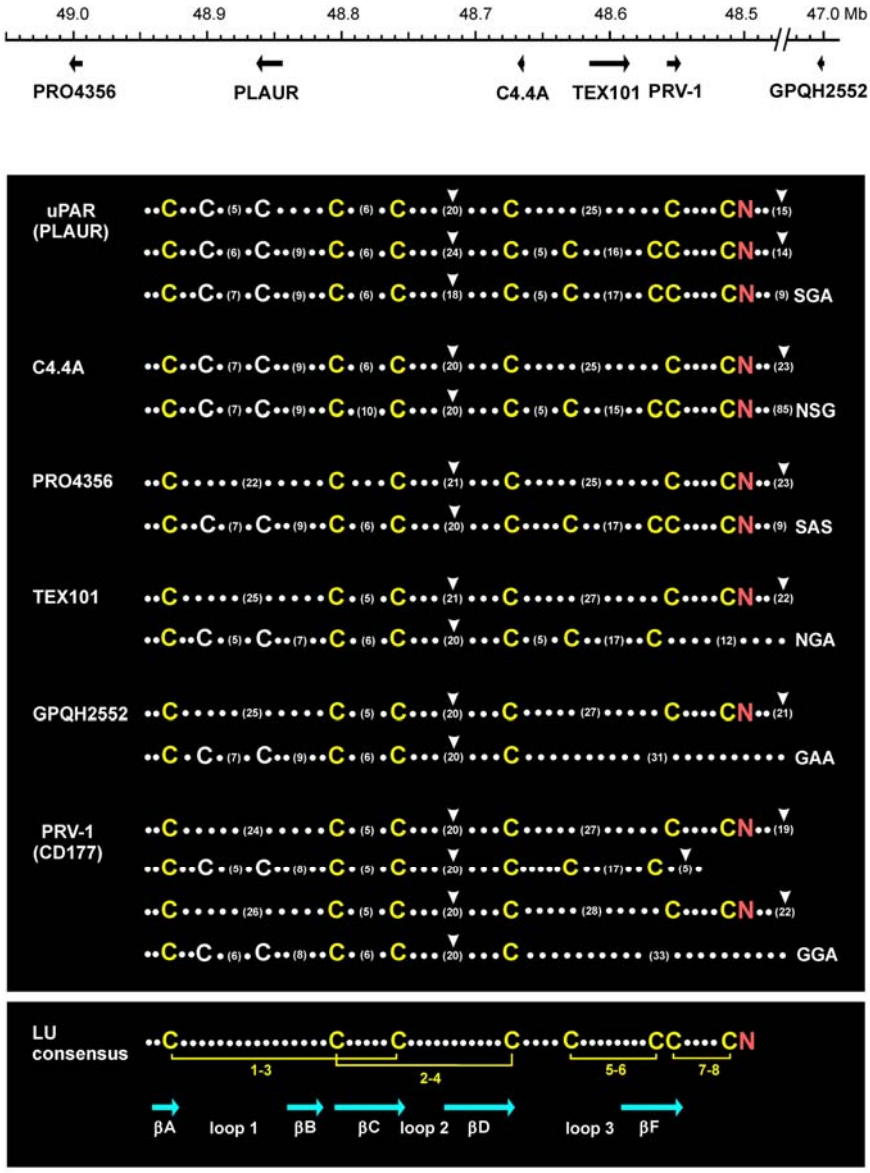

Figure 5. Presence of a uPAR-like gene cluster on human chromosome 19q13 encoding GPI-anchored proteins with multiple LU-domains. *Upper panel* shows a schematic representation of the 2Mb long region on human chromosome 19q13 that harbours at least 6 genes predicted to encode different GPI-anchored proteins containing more than one LU-domain. The predicted domain organization of these 6 multidomain proteins is shown schematically in the *lower panel*. Residues belonging to the LU consensus sequence are shown in the single letter code with conserved cysteine residues in yellow and the invariant asparagine in red. Also shown are non-consensus cysteines and the putative processing site for GPI-anchoring in white. Distances between cysteines are represented by dots, but longer distances are represented by the numbers shown in brackets. It is noteworthy that all intron boundaries are invariably found in regions encoding either the interdomain linker regions or the tip of loop 2 in the individual LU-domains, as indicated by white arrowheads.

is found at the base of loop 3 (Figure 5). The equivalent disulfide bonds in the single LU-domain proteins CD59 and *kappa*-bungarotoxin are essential for their correct folding (72, 73). Although the apparent correlation between the lack of this particular disulfide bond and the repetition of the LU-domain within these multidomain proteins could merely reflect their evolutionary relatedness, it may, however, also reflect a structural aspect of the multidomain assembly in these proteins (as discussed later).

4.3. Three-dimensional structure of human uPAR

Despite a huge research effort, the first experimentally determined X-ray structure of uPAR was not published until 2005 (43). The structure was solved for

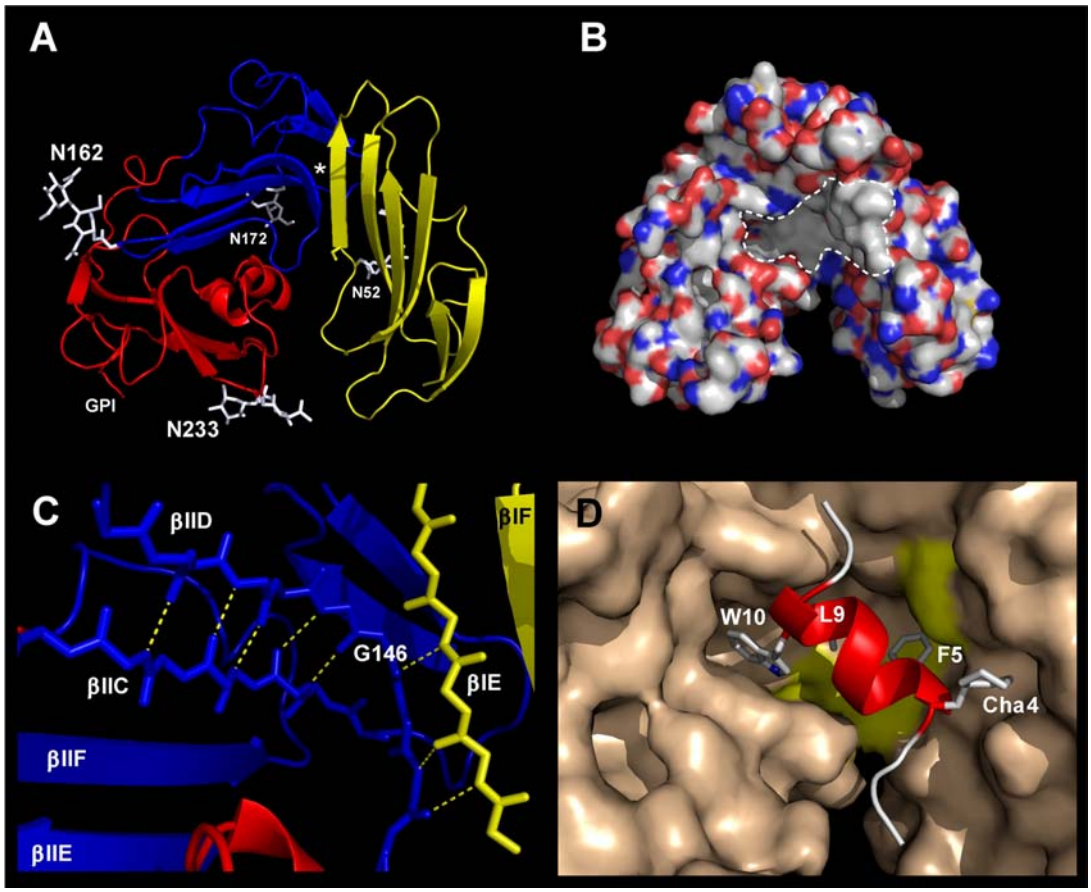

Figure 6. Crystal structure of uPAR. *Panel A* shows a ribbon diagram of the structure of human uPAR. The three domains of uPAR cooperate to form one continuous 13-stranded bent *beta*-sheet. uPAR domains DI (*yellow*), DII (*blue*) and DIII (*red*) are shown in ribbon diagrams with the proximal two N-acetyl-glucosamine moieties (*white sticks*) that were defined by the electron density (pdb:1YWH). In this structure, Asn^{233} is exceptionally exploited for glycosylation as the structure was solved for a Asn^{200}→Gln uPAR mutant with an altered processing of its potential glycosylation sites (42, 43). The asterisk marks the twined interaction of the *beta*-strand *beta*IID with *beta*IE and *beta*IIC. *Panel B* shows the equivalent surface representation of uPAR using the following colour coding: carbon and hydrogen (*gray*), oxygen (*red*), nitrogen (*blue*) and sulphur (*yellow*). The distinct and coherent grey pocket, which in this illustration is circumscribed by a white hatched line, represents the hydrophobic binding cavity in uPAR with a high density of exposed aliphatic groups. *Panel C* is a close-up of the hinge region between DI and DII, which is centred on the split interaction of the bent *beta*IID with *beta*IE and *beta*IIC. The position of Gly^{146} is highlighted. *Panel D* illustrates the uPAR-bound peptide antagonist AE147 having the sequence K-S-D-Cha-F-s-k-Y-L-W-S-S-K. The receptor is shown in a surface representation in *wheat*, whereas the peptide antagonist is represented by a ribbon diagram with side chains important for uPAR binding as white sticks. The antagonist peptide contacts part of a hydrophobic patch and sequesters it from the solvent.

a complex between a soluble version of human uPAR expressed in S2 cells and a high-affinity linear peptide antagonist of uPA binding developed by combinatorial chemistry (87). Reassuringly, this crystal structure confirmed and further substantiated the proposition advanced 11 years before (64) that uPAR consists of three homologous LU-domains each adopting the expected three-finger fold (Figure 3). In this structure, uPAR domains I and II each possess six *beta*-strands, whereas domain III only has 5, as an *alpha*-helix occupies the one side of loop 3 in this domain (*alpha*IIIE). The assembly of the multidomain structure of uPAR is accomplished by extensive *beta*-strand interactions between the individual domains, creating a large continuous 13-strand antiparallel *beta*-sheet, which bends into a croissant-like topology (Figure 6A and B). In particular, the unusual bending of the *beta*IID strand, which is centered on Gly^{146}, enables a shared interaction with *beta*-strands in both DI (*beta*IE) and DII (*beta*IIC), as illustrated in Figure 6C. An equivalently organized interface is also created between uPAR DII and DIII by the engagement of the analogous *beta*-strands, *i.e.* a bent *beta*IIE and *beta*IIID. The first loops in DII and DIII do not participate in the formation of the large central *beta*-sheet, as their *beta*-strands form two separate sheets (*beta*IIA-*beta*IIB and *beta*IIIA-*beta*IIIB). Nevertheless, more than 1000 $Å^2$ of the total DI-DII interface is provided by residues 94-115, located in the small detached *beta*-sheet formed by *beta*IIA and *beta*IIB.

As mentioned previously, the N-terminal uPAR DI lacks a particular disulfide bond that links cysteines 5-6 in the consensus for the LU-domain and which is considered indispensable for the correct folding of the single domain proteins (72, 73). As illustrated in Figure 3B, the C^{alpha} atoms of Thr^{51} and Val^{70}, which occupy the positions equivalent to those of the missing consensus cysteines, are only 6 Å apart, which is within the range that can be accommodated by a disulfide bond. Although the side chain of Thr^{51} is rotated away from uPAR DI towards DII, it nevertheless seems plausible that the molecular architecture of uPAR would actually allow this disulfide to be formed. It is, however, noteworthy that introduction of this disulfide bond might significantly influence the dynamics of the interactions between DI and DII, since it would be located at the base of the third finger linking *beta*IE and *beta*IF. This loop provides the main interface with domain II, where *beta*IE in particular engages the bent *beta*IID joining the central *beta*-sheets of these two domains (43).

The croissant-like overall folding topology of the multidomain uPAR creates an "asymmetric" globular structure, where the convex outer surface of the large central *beta*-sheet harbours the five potential N-linked glycosylation sites (shown as white sticks in Figure 6A). Intriguingly, the concave side of the central *beta*-sheet forms a relatively large and conspicuous cavity, which is approximately 19 Å deep and involves elements from all 3 LU-domains (Figure 6B). The bottom of this cavity is lined with a hydrophobic surface dominated by exposed aliphatic side chains residing in DI and DII, *i.e* Ile^{28}, Val^{29}, Leu^{31}, Leu^{38}, Leu^{40}, Leu^{55}, Leu^{66}, Leu^{123}, Val^{125}, Leu^{144}, Leu^{150} and Leu^{168} (Figure 6B). The antagonist peptide, which was instrumental for solving the initial crystal structure of uPAR (43), is efficiently embedded in the central cavity, where it buries approximately 2000 $Å^2$ of the solvent accessible receptor surface (Figure 6D). The pronounced hydrophobicity of this receptor-ligand interface is likely to contribute significantly to the subnanomolar affinity and in particular the low off-rates determined for the AE105-uPAR complex, which is comparable to that of the cognate protein ligand, uPA (87, 88). Further substantiating the importance of this cavity in uPAR is the early observation that the extrinsic fluorophore 8-anilino-1-naphthalene sulfonate (ANS) binds a hydrophobic, surface-exposed site on uPAR, which is only available in the intact, unoccupied receptor (58). The unique topology of the ligand-binding cavity in uPAR combined with certain structural similarities between the bound peptide and the receptor-binding module of uPA allowed the modelling of a uPAR-GFD complex in which the hydrophobic receptor cavity is occupied by the *beta*-hairpin of GFD (43). The overall topology of this model was later confirmed when the structure of the ATF-uPAR complex was solved by X-ray crystallography (44, 45), as discussed in section 5.1.2. From the overall topology of the uPAR-peptide complex, it is doubtful whether this structure is indeed identical to that of the unoccupied receptor, as the entropic costs of maintaining such a large solvent-exposed, hydrophobic binding site is considerable (Figure 6B). It has accordingly been speculated that unoccupied uPAR undergoes some kind of rearrangement to shield the vacant ligand-binding cavity (89). Some residual surface exposure of this cavity is nevertheless maintained in the ligand-free receptor, as assessed by the ANS fluorescence properties of purified recombinant uPAR (58) and by the observation that Tyr^{57} in the cavity is readily modified by tetranitromethane in the unoccupied receptor (90).

5. STRUCTURAL BASIS FOR LIGAND BINDING TO uPAR

A relatively large number of potential biological ligands for uPAR have been identified using a plethora of different detection methods. Besides the *bona fide* high-affinity protease ligand uPA, which provided the name for uPAR, several other possible interaction partners have been reported. These include such functionally diverse proteins as: vitronectin (91, 92), the integrins $alpha_5beta_1$, $alpha_Mbeta_2$, $alpha_3beta_1$ and $alpha_vbeta_3$ (93-97), the endocytic collagen receptor uPARAP/Endo180 (98), the activated extrinsic coagulation factor kininogen HK_a (99) and the G-coupled FPRL1 receptor (62). The present review will, however, mainly focus on structural aspects of uPA and vitronectin binding to uPAR as these two interactions are the only ones that have been characterized in detail at the molecular level.

5.1. The uPA-uPAR interaction

The interaction between uPAR and uPA or its zymogen prouPA is relatively tight with a K_D of 0.2-1 nM (100), and this interaction is now thoroughly characterized both functionally and structurally. The overall topology of the bimolecular complex allows receptor-bound prouPA to be activated by plasmin, albeit this occurs with a slightly lower efficiency when comparing preformed soluble uPAR-prouPA complexes with free prouPA (101). Importantly, these studies also demonstrate that the zymogenicity of prouPA is not altered as a consequence of uPAR binding (101), and uPAR does therefore not function as a cofactor for prouPA in strict molecular terms as do streptokinase and staphylokinase for plasminogen activation (102). In the following section, the structure of uPA will be briefly reviewed with special emphasis on its interaction with uPAR.

5.1.1. Structure of uPA

The modular serine protease uPA is secreted as a 411 residues long single-chain zymogen (prouPA), which can be activated by *e.g.* plasmin to a two-chain active protease by a single specific cleavage after Lys^{158}. The modular N-terminal region of uPA is composed of two structural domains, *i.e.* the N-terminal growth factor-like domain (GFD, residues 1-48) and a kringle domain (residues 49-131), followed by a connective peptide (residues 132-158) harbouring the activation site. For historical reasons, the modular part of uPA is denoted the amino terminal fragment (ATF) as this fragment can be generated spontaneously in purified prouPA preparations by various protease impurities (103). The C-terminal serine protease domain of uPA (residues 159-411) adopts the archetypical trypsin-like fold (104), where the interface between two symmetrical 6-stranded *beta*-barrels harbours

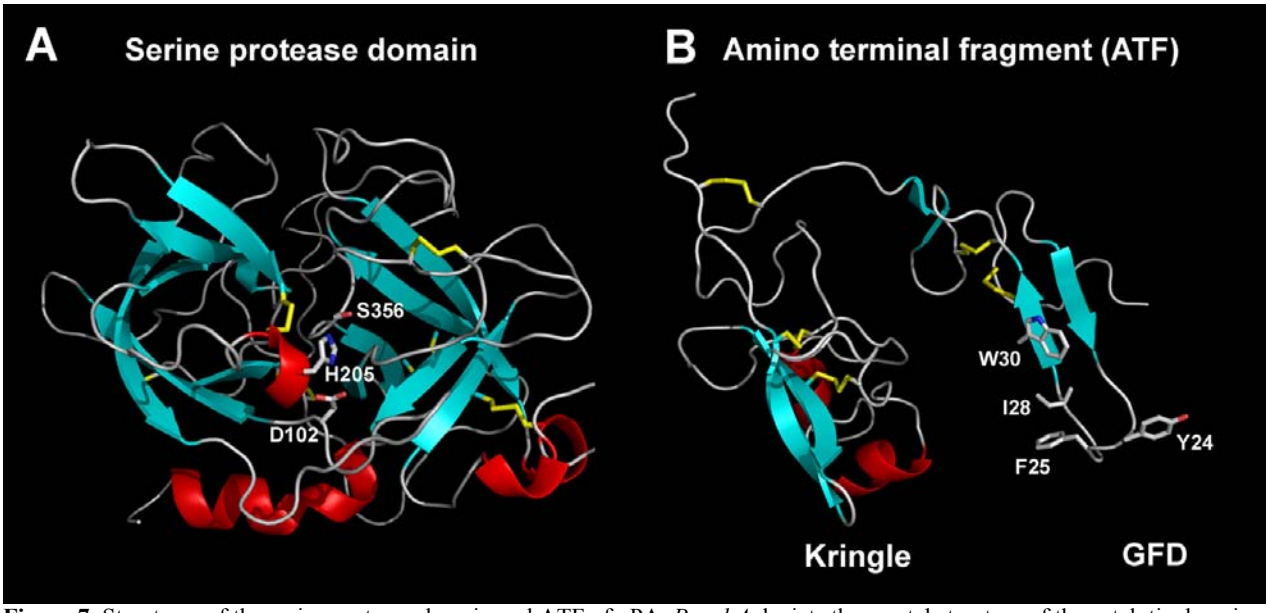

Figure 7. Structures of the serine protease domain and ATF of uPA. *Panel A* depicts the crystal structure of the catalytic domain of uPA (pdb: 1LMW) as a ribbon diagram with disulfide bonds shown as yellow sticks (104). Residues of the catalytic triad are illustrated by sticks. *Panel B* shows the solution structure of ATF in a ribbon diagram representation (pdb: 1URK). The side chains that have been determined to be important for binding to uPAR are highlighted, *i.e.* Tyr^{24}, Phe^{25}, Ile^{28} and Trp^{30} in GFD.

the catalytic triad (Asp^{102}, His^{205} and Ser^{356}), as shown in Figure 7A. Extensive structure-activity relationship studies have been performed to optimize the interaction between small organochemicals or peptide-based antagonists and the substrate recognition subsites in uPA (105, 106).

The main determinants for the interaction between uPAR and uPA reside in the N-terminal GFD, which maintains a high-affinity interaction with uPAR as an independent module (100, 107). Studies by chemical protection, site-directed mutagenesis and synthetic peptides reveal that the central *beta*-hairpin and in particular Lys^{23}, Tyr^{24}, Phe^{25}, Ile^{28} and Trp^{30} in GFD are involved in the interaction with uPAR (65, 90, 107-110). No experimental structure of two-chain uPA or prouPA has been reported, but the structures of the isolated serine protease domain (104) and ATF have been solved (45, 111), as illustrated in Figure 7A & B. Biophysical studies performed on intact uPA by NMR and differential scanning calorimetry suggest that the GFD and kringle domains have a high degree of motional freedom relative to the serine protease domain and that these domains denature independently (112-114). Accordingly, the solution structure of ATF shows few interactions between the kringle domain and GFD (111). This proposition was further consolidated by studies on the NMR relaxation properties of the molecule, demonstrating that the domains tumble independently (115). Surprisingly, the crystal structures subsequently solved for free ATF as well as for ATF in complex with uPAR both revealed an unexpected interaction between GFD and the kringle through a distinct hydrophobic interface (44, 45). What is the significance of this apparent inconsistency? A closer examination of the original data used to solve the solution structure of ATF indicated the existence of a transient interdomain interaction, since three long range interactions were recorded between Ile^{44} in GFD and Tyr^{101} in the kringle (111), and these residues are indeed located at the domain interface identified by the crystal structures of ATF (44, 45). The inconsistency between the reported NMR and X-ray structures for ATF can therefore be rationalized by the proposition that both states of ATF are populated in solution, but crystallization locks the domains into the least dynamic of their states, where the kringle domain and the growth factor domain interact through a hydrophobic interface.

5.1.2. Structure of ATF-uPAR

The structure of uPAR in complex with ATF was reported in 2006 by two independent groups, thus providing valuable insights into the molecular basis for the high affinity of the ATF-uPAR interaction (44, 45). The complex was initially crystallized in the presence of a Fab fragment from a monoclonal anti-uPAR antibody having its epitope localized on uPAR DIII (116). The structure solved for this ATF-uPAR-Fab complex was subsequently recapitulated by an independent study on a bimolecular ATF-uPAR complex (45). In accordance with initial modeling studies (43, 117), the crystal structures solved for the ATF-uPAR complexes clearly show that the *beta*-hairpin of GFD inserts deeply into the central cavity of the receptor, where it engages and completely shields the hydrophobic surface lining of the cavity (Figure 8A). A total of 1171 $Å^2$ of solvent-accessible surface area in uPAR is buried at the interface upon complex formation (44). The ATF-uPAR interface defined by the crystal structure harbours most of the residues previously identified as being functionally important for the thermodynamics of the interaction by site-directed mutagenesis, *i.e.* Lys^{23}, Tyr^{24},

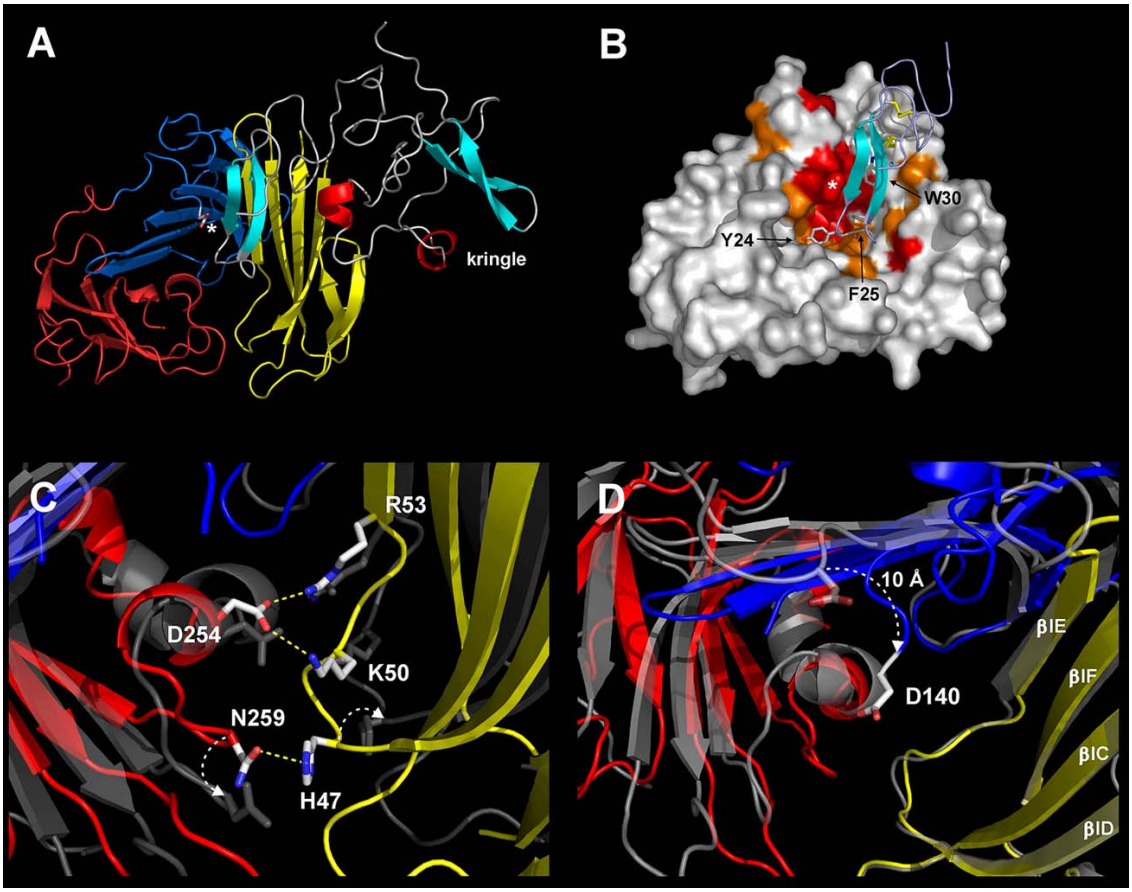

Figure 8. Structure of ATF-uPAR complex. The crystal structure solved for the ATF-uPAR complex is shown in *panel A* as a ribbon diagram representation (pdb: 2FD6) (44). The position of Asp[140] is indicated by the asterisk, and the color coding for the individual uPAR domains is identical to the one used in Figure 6. A surface representation of uPAR with the bound GFD as a ribbon diagram is shown in *panel B*. Residues in uPAR contributing to the energetics of the complex formation are shown in red (change larger than 1 kcal/mol) and orange (change between 0.5 and 1 kcal/mol), as assessed by alanine scanning mutagenesis (117). Again the position of Asp[140] in the loop connecting *beta*IIC and *beta*IID is identified by an asterisk. Superimpositions of the structures solved for the two different uPAR complexes are shown in *panels C & D*, where the ribbon diagram representing the peptide complex is shown in transparent dark grey. The structures were superimposed on DII in *panel C* and on DI in *panel D*. The closure of the breach between DI and DIII is illustrated in *panel* C with the established interdomain contacts highlighted by the hydrogen bonding between the relevant amino acids shown as dashed lines. The repositioning of Asp[140] is shown in *panel D*.

Phe[25], Ile[28] and Trp[30] in uPA (108), Arg[25], Thr[27], Leu[40], Lys[50], Arg[53], Leu[55], Tyr[57] and Leu[66] in uPAR DI, and Val[125], Thr[127], Asp[140], Asp[141], Leu[150], Pro[151] and Leu[168] in uPAR DII, as illustrated in Figure 8B (46, 117).

As opposed to the intimate engagement of GFD in receptor binding, the crystal structures also reveal that the kringle domain of uPA only loosely docks against uPAR DI outside the central cavity, where His[87] in the kringle forms van der Waals contact with Asp[11] in uPAR (44). Neither this interaction nor the intramolecular interaction between the kringle and GFD modules described previously seem, however, to contribute significantly to the kinetics of the ATF-uPAR interaction, as only moderate changes in the kinetic rate constants could be revealed for the binding of GFD and ATF to uPAR^{wt} or uPAR^{D11A} by surface plasmon resonance (100, 117). Nonetheless, one report seems to argue for an undefined "stabilizing" role of the kringle domain in the uPA-uPAR interaction (118). The spatial proximity between the kringle domain in uPA and uPAR DI is actually exploited by the widely used chemical cross-linking assay for detection of uPAR using ^{125}I-labelled ATF and amine reactive, homobifunctional cross-linkers (37-39, 47, 48, 117). Studies on the impact of individually replacing all lysine residues present in either uPAR or ATF by alanine demonstrate that the specific target sites of these chemical cross-linkers are Lys[43] in uPAR and Lys[98] in uPA (117). The distance of 10.8 Å between the corresponding target *episilon*-amino groups in the ATF-uPAR is well within the range of the employed cross-linkers. The failure of detecting the orthologous murine complexes by this method is accounted for by the replacement of this particular Lys[43] by arginine in mouse uPAR (117).

Intriguingly, the crystal structures solved for uPAR complexes with either the peptide antagonist or ATF display notable differences, which could have a bearing on the dynamic assembly of the multidomain receptor. Superimposition of the two structures reveals that the open croissant-like topology of uPAR in the peptide complex is transformed into a more closed and condensed structure in the ATF-uPAR complex (44). This is in part accomplished by an approximately 20 degree rotation of DI towards DII+DIII in the ATF-uPAR complex. As a consequence, the breach observed between uPAR DI and DIII in the peptide complex undergoes a closure in the ATF complex, and new interdomain contacts are now being established between the side chains of Lys^{50} and Arg^{53} in DI to Asp^{254} in DIII as well as between His^{47} in DI and Asn^{259} in DIII (Figure 8C). The magnitude of this movement is illustrated by the difference in the $N^{epsilon2}$-O^{delta1} distances between His^{47} and Asn^{259} in the two complexes, which is 2.9 Å in the ATF complex (44) compared to 12.1 Å in the peptide complex (43). Another noteworthy difference between these structures is the repositioning of Asp^{140} situated in the loop between *beta*IIC and *beta*IID, which moves approximately 10 Å towards the entrance of the central binding cavity in the ATF complex (Figures 8B & 8D). Here, Asp^{140} forms a hydrogen bond to Ser^{21} in GFD, and the loop closes the occupied ligand-binding cavity like a lid (44). The functional importance of this particular residue is implicated by the huge impact on k_{off} recorded for the prouPA-$uPAR^{D140A}$ complex by surface plasmon resonance (117).

A thorough kinetic study on the prouPA-uPAR interaction using a library of purified single-site alanine mutants of uPAR has provided a valuable functional correlation to the solved crystal structures (117). First and foremost, this study identified those residues in the binding cavity (*i.e.* structural epitope) that actually provide a thermodynamic contribution to uPA binding (*i.e.* functional epitope), which is illustrated in Figure 8B. As a valuable spin-off from these experiments, the alanine scanning mutagenesis also provides some information on the interdomain stability in uPAR. Analysis of uPA binding to these single-site uPAR mutants identified several receptor residues that are sensitive to alanine replacements, but do not contact uPA directly in the crystal structure. These residues probably have an indirect effect on the topology of the binding cavity by stabilizing the multidomain structure of uPAR. In line with this argument, residues buried at the interface between uPAR DI and DII are often particularly sensitive to alanine mutations, *e.g.* those located in the *beta*-hairpin formed by *beta*IIA and *beta*IIB (*i.e.* Ser^{97}, Asp^{102}, Ser^{104} and Leu^{113}) or in the aforementioned bent *beta*IID strand (*i.e.* His^{143}, Leu^{144}, Arg^{145}, Gly^{146} and Gly^{148}). Maintenance of high-affinity uPA binding is therefore tightly linked to the correct assembly of the interface between DI and DII. Examination of the corresponding interface between uPAR DII and DIII reveals that this interaction is much more resilient to single-site mutagenesis, suggesting that uPA binding is less dependent on subtle changes in the relative orientation of these two domains. This proposition is in accordance with the observation that none of the residues in uPAR DIII have a significant impact on the kinetics of the prouPA-uPAR interaction when mutated individually to alanine (117).

5.2. The vitronectin-uPAR interaction

The extracellular matrix glycoprotein vitronectin represents another well-characterized protein ligand for uPAR. The first indication for a functional relationship between these two proteins came from the observation that cytokine-stimulated human myeloid cells up-regulate uPAR and adhere to serum-coated surfaces in a uPA-dependent manner (119). It was subsequently demonstrated that uPAR interacts directly with the matrix form of vitronectin, independent of any integrin involvement as the adherence persists in the presence of EDTA and RGD peptides (91, 92). Importantly, it was further demonstrated both in cell adhesion assays and in purified systems that the uPAR-vitronectin interaction is regulated by the receptor occupancy with prouPA (59, 91, 120-123). Maintenance of the multidomain structure of uPAR is hence a prerequisite for its interaction with vitronectin, as outlined previously for uPA binding (51). From a functional point of view, several studies using uPAR-transfected cell lines have demonstrated that the uPAR-vitronectin interaction elicits pronounced alterations in cell morphology and activation of signal pathways leading to increased cell adhesion and migration (124, 125). In primary human microvascular endothelial cells, this interaction is also of functional significance, as uPAR and prouPA co-localize at focal adhesion sites in a vitronectin-dependent process (126).

5.2.1. Structure of the SMB domain of vitronectin

Vitronectin is a 75 kDa adhesive glycoprotein, which is found as an abundant soluble protein in plasma (5 micromolar) as well as a sequestered form in the extracellular matrix, where it provides a functional interactive surface. This extended matrix form of vitronectin binds a number of different ligands including integrins, PAI-1, uPAR, uPA, plasminogen and heparin (127). The single-chain vitronectin is composed of an NH_2-terminal somatomedin B domain (SMB, residues 1-44), followed by a long connecting peptide (CP, residues 45-131) harbouring the integrin binding signature Arg-Gly-Asp^{47} and finally two hemopexin-like domains (HP, residues 131-459), as shown schematically in Figure 9A. So far, no experimental high-resolution structure for intact vitronectin has been solved, but modelling studies have been attempted using low resolution data from small-angle X-ray scattering and computational threading, which portray vitronectin as a 110 Å elongated peanut-shaped molecule (128). Although the small NH_2-terminal SMB domain has been studied extensively as an isolated fragment, a significant ambiguity nevertheless exists in the literature regarding its disulfide pairing (129-133) and its three-dimensional structure (134-137). This controversy appears, however, now to be resolved by comparing the function and stability of plasma vitronectin-derived SMB with that of chemically synthesized SMB variants with predefined disulfide connectivities (132) using hydrogen-deuterium exchange and NMR (135). These studies corroborate the original disulfide connectivity and protein structure of SMB that were derived by X-ray

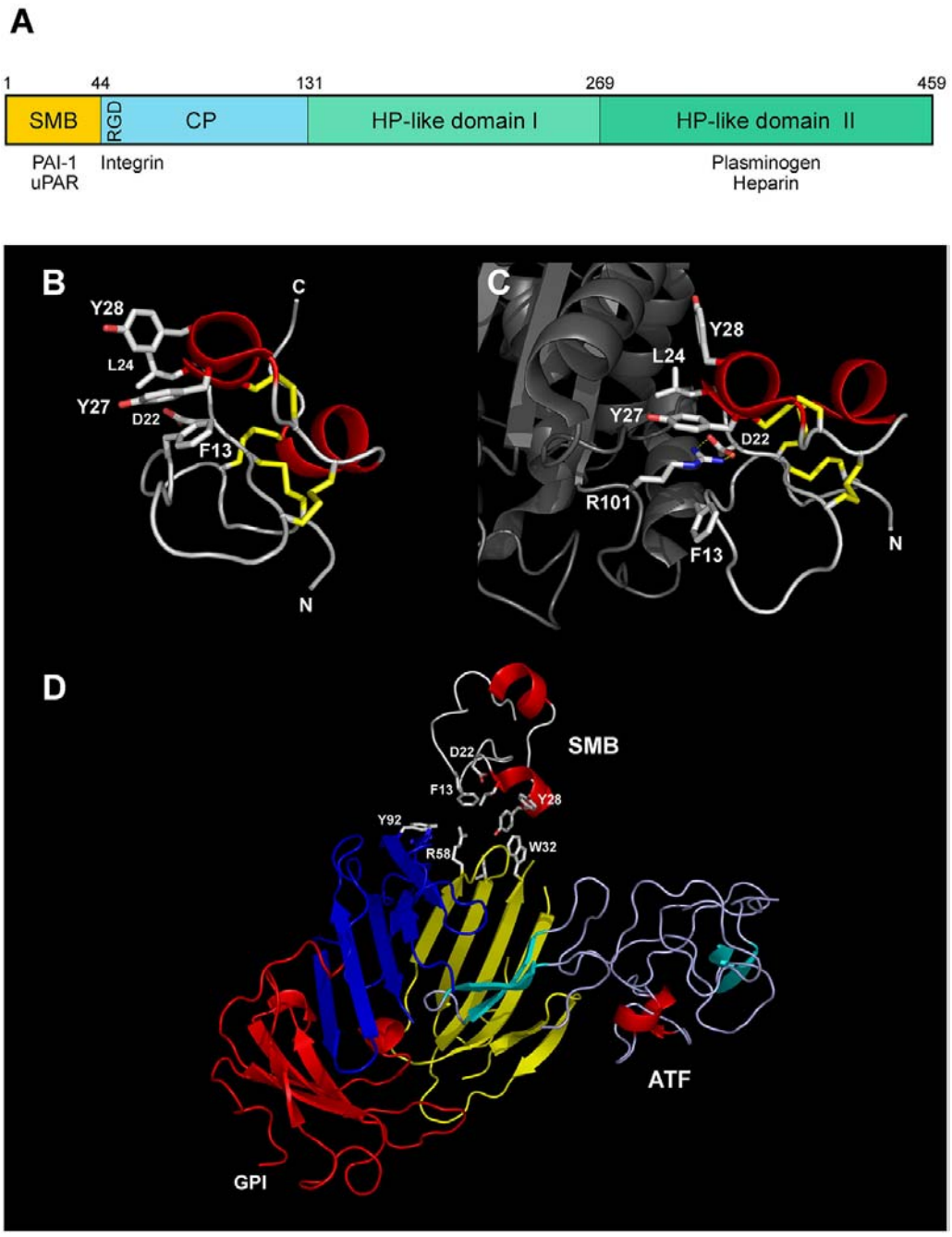

Figure 9. Model of the SMB-uPAR-ATF complex. The domain organization of human full-length vitronectin is illustrated schematically in *panel A* by the bar, where the positions of epitopes for selected ligands are roughly indicated. *HP* is hemopexin and *CP* is connecting peptide. *Panel B* shows the solution structure of SMB (pdb: 2JQ8) as a ribbon diagram. The 4 disulfide bonds are shown as yellow sticks. Residues involved in PAI-1 and uPAR binding are shown as white sticks, and they form a small surface-exposed hydrophobic cluster. The molecular interface between PAI-1 (in grey) and SMB is shown in *panel C* as a ribbon diagram with essential amino acids shown as sticks (pdb: 1OC0). The distinct ionic interaction between Arg^{101} in PAI-1 and Asp^{22} in SMB is highlighted. A manual docking model of the SMB-uPAR-ATF complex based on the identification of the complementary functional epitopes in SMB and uPAR is shown in *panel D* (122) using the pdb coordinates 2FD6 and 1OC0. This model suggests the absence of a direct interaction between the kringle of uPA and SMB in the ternary complex.

crystallography for an SMB-PAI-1 complex (137). SMB folds into a roughly globular module with little secondary structure, but having a tightly disulfide crosslinked core (Figures 9B and 9C).

A non-exhaustive alanine scanning mutagenesis of the SMB domain identified the functional epitope for the SMB-uPAR interaction, and it includes residues Phe^{13}, Asp^{22}, Leu^{24}, Tyr^{27} and Tyr^{28} (122, 138). These residues form a compact, hydrophobic epitope on the surface of the unbound SMB domain, as shown in Figure 9B. Intriguingly, the same residues have been found to be important for PAI-1 binding (138), and the structure solved for the SMB-PAI-1 complex reveals that these residues are indeed located at the intermolecular interface (137). A noticeable property of this interface is the ionic bond formed between Asp^{22} in SMB and Arg^{101} in PAI-1, where the methylene groups of Arg^{101} are shielded by the aromatic side chains of Phe^{13} and Tyr^{28} in SMB. In accordance with the significant overlap of the functional epitopes on SMB for uPAR and PAI-1 binding, it has been demonstrated that PAI-1 efficiently competes uPAR binding to vitronectin (51, 139). Along the same lines, it has been demonstrated that PAI-1 also inhibits integrin-mediated cell adhesion by binding to the SMB domain and thereby sterically constraining the accessibility to the adjacent RGD motif (140).

5.2.2. Model of the ATF-uPAR-SMB

So far, no crystal structures for the ATF-uPAR-SMB complex has been reported. As alluded to above, the binding epitope for uPAR on vitronectin resides primarily on the SMB domain, and the involved residues have been identified by site-directed mutagenesis and are highlighted in Figure 9B (122, 138, 141). The corresponding binding interface for vitronectin on human uPAR was identified by exhaustive site-directed mutagenesis interrogating 244 individual positions in the receptor for their importance in vitronectin binding of preformed prouPA-uPAR complexes (122). Only 5 out of the 244 positions tested in uPAR were defined as contributing significantly to the thermodynamics of the prouPA-uPAR-vitronectin interaction, and reassuringly, they all cluster in a coherent, surface-exposed site located outside the interface occupied by ATF, i.e. Trp^{30}, Arg^{58} and Ile^{63} in DI, as well as Arg^{91} and Tyr^{92} in the linker region connecting DI and DII. The composite nature of this binding site provides a straightforward explanation for the sensitivity of vitronectin binding to cleavage of the linker region between uPAR DI and DII (51). Equilibrium binding studies by surface plasmon resonance emphasize the importance of these residues in the interaction with the isolated SMB domain as well, suggesting that this site primarily interacts with SMB. Identification of the two complementary functional epitopes in the uPAR-SMB complex thus enables a tentative positioning of the SMB domain onto the crystal structure of the uPAR-ATF complex, as illustrated in Figure 9D (122). Such preliminary docking experiments suggest that a direct interaction between Arg^{91} in uPAR and Asp^{22} in the SMB domain is indeed possible and that the intermolecular interface may to some extent resemble that of the SMB-PAI-1 complex. Nonetheless, it should be emphasized that the affinity of the two interactions are vastly different as the KD for PAI-1 is 0.3 nM (141), compared to 1.9×10^3 nM for uPAR (122).

It has been reported by several groups that the interaction between uPAR and vitronectin to a large extent is controlled by the receptor occupancy with prouPA (91, 122, 123). Full-length uPA and ATF, but not GFD, were found to enhance the affinity of uPAR for immobilized vitronectin using purified components, suggesting a possible role of the kringle domain of uPA in this interaction. Inspection of our docking model for the trimolecular ATF-uPAR-SMB complex does not, however, support the proposal of an additional contribution to the affinity by a direct interaction between the bound SMB and the kringle domain of uPA (Figure 9D). Accordingly, we find that the affinity for the SMB domain alone is indeed increased 4-5 fold by saturation of uPAR with either prouPA or ATF, but surprisingly, GFD binding mounts an identical increase in the affinity for SMB (122), which is clearly different to the effects observed in the solid-phase binding assay using full-length immobilized vitronectin (122, 123). It could therefore be speculated that prouPA and ATF may contain an additional binding site for vitronectin that is located outside the SMB domain. Such a secondary interaction has been reported previously, but has not been substantiated beyond the initial report (142).

6. CONCLUSIONS AND FUTURE PERSPECTIVES

With the access to the crystal structures solved for uPAR in complex with ATF and a linear peptide antagonist, the molecular basis for the interaction between uPAR and its potential protein ligands can be explored with much more confidence. In particular, the often inconsistent data obtained previously from diverse functional studies on specified uPAR mutants can now be evaluated in a much more rigorous structural context. One of the central structural issues that still remains to be solved is the structure of the unoccupied uPAR to delineate how this receptor thermodynamically can accommodate such a large and empty hydrophobic binding cavity. Another important aspect is the structure of the prouPA-uPAR complex with special emphasis on the position of the activation site of uPA relative to the receptor. With a view to the numerous potential binding partners proposed for uPAR, it will also be important to obtain more consistent structural data on these interactions to allow their rational manipulation in a well-defined functional and structural setting. Such knowledge will be essential for the rational development of specific drug candidates targeting uPAR during cancer patient management.

7. ACKNOWLEGMENTS

The assistance of John Post (Finsen Laboratory) in creating the artwork is greatly appreciated. This work was supported by the European Commission, grant LSHC-CT-2003-503297. All graphic representations of protein structures were created by PyMol (DeLano Scientific)

8. REFERENCES

1. Page-McCaw, A., Ewald, A.J. & Werb, Z.: Matrix metalloproteinases and the regulation of tissue remodelling. *Nat Rev Mol Cell Biol*, 8, 221-33 (2007)

2. Dano, K., Behrendt, N., Hoyer-Hansen, G., Johnsen, M., Lund, L., Ploug, M. & Romer, J.: Plasminogen activation and cancer. *Thromb Haemost.*, 93, 676-81 (2005)
3. Romer, J., Bugge, T., Pyke, C., Lund, L., Flick, M., Degen, J. & Dano, K.: Impaired wound healing in mice with a disrupted plasminogen gene. *Nat Med.*, 2, 287-92 (1996)
4. Lund, L., Green, K., Stoop, A., Ploug, M., Almholt, K., Lilla, J., Nielsen, B., Christensen, I., Craik, C., Werb, Z., Dano, K. & Romer, J.: Plasminogen activation independent of uPA and tPA maintains wound healing in gene-deficient mice. *EMBO J.*, 25, 2686-97 (2006)
5. Ellis, V., Scully, M.F. & Kakkar, V.V.: Plasminogen activation initiated by single-chain urokinase-type plasminogen activator. Potentiation by U937 monocytes. *J Biol Chem*, 264, 2185-8 (1989)
6. Ellis, V. & Dano, K.: Potentiation of plasminogen activation by an anti-urokinase monoclonal antibody due to ternary complex formation. A mechanistic model for receptor-mediated plasminogen activation. *J. Biol. Chem.*, 268, 4806-4813 (1993)
7. Kobayashi, H., Schmitt, M., Goretzki, L., Chucholowski, N., Calvete, J., Kramer, M., Günzler, W., Janicke, F. & Graeff, H.: Cathepsin B efficiently activates the soluble and the tumor cell receptor-bound form of the proenzyme urokinase-type plasminogen activator (ProuPA). *J. Biol. Chem.*, 266, 5147-5152 (1991)
8. Lee, S.-L., Dickson, R.B. & Lin, C.-Y.: Activation of Hepatocyte Growth Factor and Urokinase/Plasminogen Activator by Matriptase, an Epithelial Membrane Serine Protease *J. Biol. Chem.*, 275, 36720-36725 (2000)
9. Kilpatrick, L.M., Harris, R.L., Owen, K.A., Bass, R., Ghorayeb, C., Bar-Or, A. & Ellis, V.: Initiation of plasminogen activation on the surface of monocytes expressing the type II transmembrane serine protease matriptase *Blood*, 108, 2616-2623 (2006)
10. Moran, P., Li, W., Fan, B., Vij, R., Eigenbrot, C. & Kirchhofer, D.: Pro-urokinase-type Plasminogen Activator Is a Substrate for Hepsin. *J. Biol. Chem.*, 281, 30439-30446 (2006)
11. Lijnen, H.: Gene targeting in hemostasis. alpha$_2$-antiplasmin. *Front Biosci.* 6, D239-47 (2001)
12. Ragno, P.: The urokinase receptor: a ligand or a receptor? Story of a sociable molecule. *Cellular and Molecular Life Sciences (CMLS)*, 63, 1028-1037 (2006)
13. Blasi, F. & Carmeliet, P.: uPAR: A verstile signalling orchestrator. *Nat Rev Mol Cell Biol*, 3, 932-943 (2002)
14. Roldan, A., Cubellis, M., Masucci, M., Behrendt, N., Lund, L., Dano, K., Appella, E. & Blasi, F.: Cloning and expression of the receptor for human urokinase plasminogen activator, a central molecule in cell surface, plasmin dependent proteolysis. *EMBO Journal*, 9, 467-74 (1990)
15. Engelholm, L.H. & Behrendt, N.: Differential binding of urokinase and peptide antagonists to the urokinase receptor: evidence from characterization of the receptor in four primate species. *Biol Chem*, 382, 435-42 (2001)
16. Fowler, B., Mackman, N., Parmer, R.J. & Miles, L.A.: Binding of human single chain urokinase to Chinese Hamster Ovary cells and cloning of hamster u-PAR. *Thromb Haemost*, 80, 148-54 (1998)
17. Krätzschmar, J., Haendler, B., Kojima, S., Rifkin, D.B. & Schleuning, W.D.: Bovine urokinase-type plasminogen activator and its receptor: cloning and induction by retinoic acid. *Gene*, 125, 177-83 (1993)
18. Kristensen, P., Eriksen, J., Blasi, F. & Dano, K.: Two alternatively spliced mouse urokinase receptor mRNAs with different histological localization in the gastrointestinal tract. *J Cell Biol*, 115, 1763-71 (1991)
19. Rabbani, S.A., Rajwans, N., Achbarou, A., Murthy, K.K. & Goltzman, D.: Isolation and characterization of multiple isoforms of the rat urokinase receptor in osteoblasts. *FEBS Lett*, 338, 69-74 (1994)
20. Ploug, M., Ronne, E., Behrendt, N., Jensen, A., Blasi, F. & Dano, K.: Cellular receptor for urokinase plasminogen activator. Carboxyl- terminal processing and membrane anchoring by glycosyl-phosphatidylinositol. *J. Biol. Chem.*, 266, 1926-1933 (1991)
21. Moller, L., Ploug, M. & Blasi, F.: Structural requirements for glycosyl-phosphatidylinositol-anchor attachment in the cellular receptor for urokinase plasminogen activator. *Eur J Biochem.*, 208, 493-500 (1992)
22. Eisenhaber, B., Bork, P. & Eisenhaber, F.: Post-translational GPI lipid anchor modification of proteins in kingdoms of life: analysis of protein sequence data from complete genomes *Protein Eng.*, 14, 17-25 (2001)
23. Udenfriend, S. & Kodukula, K.: How Glycosyl-Phosphatidylinositol-Anchored Membrane Proteins are Made *Annual Review of Biochemistry*, 64, 563-591 (1995)
24. Lehto, M.T. & Sharom, F.J.: Proximity of the Protein Moiety of a GPI-Anchored Protein to the Membrane Surface: A FRET Study. *Biochemistry*, 41, 8368-8376 (2002)
25. Chevalier, F., Lopez-Prados, J., Perez, S., Martín-Lomas, M. & Nieto, P.M.: Conformational Study of GPI Anchors: the Common Oligosaccharide GPI Anchor Backbone. *European Journal of Organic Chemistry*, 2005, 3489-3498 (2005)
26. Chevalier, F., Lopez-Prados, J., Groves, P., Perez, S., Martin-Lomas, M. & Nieto, P.M.: Structure and dynamics of the conserved protein GPI anchor core inserted into detergent micelles *Glycobiology*, 16, 969-980 (2006)
27. Suzuki, K.G., Fujiwara, T.K., Sanematsu, F., Iino, R., Edidin, M. & Kusumi, A.: GPI-anchored receptor clusters transiently recruit Lyn and G alpha for temporary cluster immobilization and Lyn activation: single-molecule tracking study 1. *J Cell Biol*, 177, 717-30 (2007)
28. Zhang, F., Crise, B., Su, B., Hou, Y., Rose, J., Bothwell, A. & Jacobson, K.: Lateral diffusion of membrane-spanning and glycosylphosphatidylinositol-linked proteins: toward establishing rules governing the lateral mobility of membrane proteins *J. Cell Biol.*, 115, 75-84 (1991)
29. Myohanen, H., Stephens, R., Hedman, K., Tapiovaara, H., Ronne, E., Hoyer-Hansen, G., Dano, K. & Vaheri, A.: Distribution and lateral mobility of the urokinase-receptor complex at the cell surface. *J. Histochem. Cytochem.*, 41, 1291-1301 (1993)
30. Schnitzer, J.E., McIntosh, D.P., Dvorak, A.M., J., L. & Oh, P.: Separation of caveolae from associated

microdomains of GPI-anchored proteins. *Science*, 269, 1435-1439 (1995)
31. Bohuslav, J., Horejsi, V., Hansmann, C., Stockl, J., Weidle, U., Majdic, O., Bartke, I., Knapp, W. & Stockinger, H.: Urokinase plasminogen activator receptor, beta 2-integrins, and Src- kinases within a single receptor complex of human monocytes *J. Exp. Med.*, 181, 1381-1390 (1995)
32. Stahl, A. & Mueller, B.: The urokinase-type plasminogen activator receptor, a GPI-linked protein, is localized in caveolae *J. Cell Biol.*, 129, 335-344 (1995)
33. Cunningham, O., Andolfo, A., Santovito, M.L., Iuzzolino, L., Blasi, F. & Sidenius, N.: Dimerization controls the lipid raft partitioning of uPAR/CD87 and regulates its biological functions. *EMBO J.*, 22, 5994-6003 (2003)
34. Ploug, M., Plesner, T., Ronne, E., Ellis, V., Hoyer-Hansen, G., Hansen, N.E. & Dano, K.: The receptor for urokinase-type plasminogen activator is deficient on peripheral blood leukocytes in patients with paroxysmal nocturnal hemoglobinuria. *Blood*, 79, 1447-55 (1992)
35. Hill, A., Richards, S.J. & Hillmen, P.: Recent developments in the understanding and management of paroxysmal nocturnal haemoglobinuria. *Br J Haematol*, 137, 181-92 (2007)
36. Ploug, M., Eriksen, J., Plesner, T., Hansen, N.E. & Dano, K.: A soluble form of the glycolipid-anchored receptor for urokinase-type plasminogen activator is secreted from peripheral blood leukocytes from patients with paroxysmal nocturnal hemoglobinuria. *Eur J Biochem*, 208, 397-404 (1992)
37. Nielsen, L., Kellerman, G., Behrendt, N., Picone, R., Dano, K. & Blasi, F.: A 55,000-60,000 Mr receptor protein for urokinase-type plasminogen activator. Identification in human tumor cell lines and partial purification. *J. Biol. Chem.*, 263, 2358-2363 (1988)
38. Behrendt, N., Ronne, E., Ploug, M., Petri, T., Lober, D., Nielsen, L., Schleuning, W., Blasi, F., Appella, E. & Dano, K.: The human receptor for urokinase plasminogen activator. NH2-terminal amino acid sequence and glycosylation variants. *J. Biol. Chem.*, 265, 6453-6460 (1990)
39. Estreicher, A., Wohlwend, A., Belin, D., Schleuning, W. & Vassalli, J.: Characterization of the cellular binding site for the urokinase-type plasminogen activator. *J. Biol. Chem.*, 264, 1180-1189 (1989)
40. Ploug, M., Rahbek-Nielsen, H., Nielsen, P.F., Roepstorff, P. & Dano, K.: Glycosylation Profile of a Recombinant Urokinase-type Plasminogen Activator Receptor Expressed in Chinese Hamster Ovary Cells *J. Biol. Chem.*, 273, 13933-13943 (1998)
41. Nilsson, I. & von Heijne, G.: Glycosylation Efficiency of Asn-Xaa-Thr Sequons Depends Both on the Distance from the C Terminus and on the Presence of a Downstream Transmembrane Segment *J. Biol. Chem.*, 275, 17338-17343 (2000)
42. Gardsvoll, H., Werner, F., Sondergaard, L., Dano, K. & Ploug, M.: Characterization of low-glycosylated forms of soluble human urokinase receptor expressed in Drosophila Schneider 2 cells after deletion of glycosylation-sites. *Protein Expression and Purification*, 34, 284-295 (2004)
43. Llinas, P., Le Du, M.H., Gardsvoll, H., Dano, K., Ploug, M., Gilquin, B., Stura, E.A. & Menéz, A.: Crystal structure of the human urokinase plasminogen activator receptor bound to an antagonist peptide. *EMBO J.*, 24, 1655-63 (2005)
44. Huai, Q., Mazar, A.P., Kuo, A., Parry, G.C., Shaw, D.E., Callahan, J., Li, Y., Yuan, C., Bian, C., Chen, L., Furie, B., Furie, B.C., Cines, D.B. & Huang, M.: Structure of Human Urokinase Plasminogen Activator in Complex with Its Receptor. *Science*, 311, 656-659 (2006)
45. Barinka, C., Parry, G., Callahan, J., Shaw, D.E., Kuo, A., Bdeir, K., Cines, D.B., Mazar, A. & Lubkowski, J.: Structural Basis of Interaction between Urokinase-type Plasminogen Activator and its Receptor. *Journal of Molecular Biology*, 363, 482-495 (2006)
46. Gardsvoll, H., Dano, K. & Ploug, M.: Mapping Part of the Functional Epitope for Ligand Binding on the Receptor for Urokinase-type Plasminogen Activator by Site-directed Mutagenesis *J. Biol. Chem.*, 274, 37995-38003 (1999)
47. Moller, L., Pollanen, J., Ronne, E., Pedersen, N. & Blasi, F.: N-linked glycosylation of the ligand-binding domain of the human urokinase receptor contributes to the affinity for its ligand. *J. Biol. Chem.*, 268, 11152-11159 (1993)
48. Behrendt, N., Ploug, M., Patthy, L., Houen, G., Blasi, F. & Dano, K.: The ligand-binding domain of the cell surface receptor for urokinase- type plasminogen activator. *J. Biol. Chem.*, 266, 7842-7847 (1991)
49. Ploug, M., Kjalke, M., Ronne, E., Weidle, U., Hoyer-Hansen, G. & Dano, K.: Localization of the disulfide bonds in the NH_2-terminal domain of the cellular receptor for human urokinase-type plasminogen activator. A domain structure belonging to a novel superfamily of glycolipid-anchored membrane proteins. *J. Biol. Chem.*, 268, 17539-17546 (1993)
50. Hoyer-Hansen, G., Ronne, E., Solberg, H., Behrendt, N., Ploug, M., Lund, L., Ellis, V. & Dano, K.: Urokinase plasminogen activator cleaves its cell surface receptor releasing the ligand-binding domain. *J. Biol. Chem.*, 267, 18224-18229 (1992)
51. Hoyer-Hansen, G., Behrendt, N., Ploug, M., Dano, K. & Preissner, K.T.: The intact urokinase receptor is required for efficient vitronectin binding: receptor cleavage prevents ligand interaction. *FEBS Letters*, 420, 79-85 (1997)
52. Sidenius, N., Sier, C.F.M. & Blasi, F.: Shedding and cleavage of the urokinase receptor (uPAR): identification and characterisation of uPAR fragments *in vitro* and *in vivo*. *FEBS Letters*, 475, 52-56 (2000)
53. Koolwijk, P., Sidenius, N., Peters, E., Sier, C.F.M., Hanemaaijer, R., Blasi, F. & van Hinsbergh, V.W.M.: Proteolysis of the urokinase-type plasminogen activator receptor by metalloproteinase-12: implication for angiogenesis in fibrin matrices *Blood*, 97, 3123-3131 (2001)
54. Beaufort, N., Leduc, D., Eguchi, H., Mengele, K., Hellmann, D., Masegi, T., Kamimura, T., Yasuoka, S., Fend, F., Chignard, M. & Pidard, D.: The human airway trypsin-like protease modulates the urokinase receptor (uPAR, CD87) structure and functions *Am J Physiol Lung Cell Mol Physiol*, 292, 1263-1272 (2007)
55. Beaufort, N., Debela, M., Creutzburg, S., Kellermann, J., Bode, W., Schmitt, M., Pidard, D. & Magdolen, V.: Interplay of human tissue kallikrein 4 (hK4) with the plasminogen activation system: hK4 regulates the structure

and functions of the urokinase-type plasminogen activator receptor (uPAR). *Biol Chem.*, 387, 217-22 (2006)
56. Beaufort, N., Leduc, D., Rousselle, J.-C., Magdolen, V., Luther, T., Namane, A., Chignard, M. & Pidard, D.: Proteolytic Regulation of the Urokinase Receptor/CD87 on Monocytic Cells by Neutrophil Elastase and Cathepsin G *J Immunol*, 172, 540-549 (2004)
57. Ke, S.-H., Coombs, G.S., Tachias, K., Corey, D.R. & Madison, E.L.: Optimal Subsite Occupancy and Design of a Selective Inhibitor of Urokinase *J. Biol. Chem.*, 272, 20456-20462 (1997)
58. Ploug, M., Ellis, V. & Dano, K.: Ligand Interaction between Urokinase-Type Plasminogen Activator and Its Receptor Probed with 8-Anilino-1-naphthalenesulfonate. Evidence for a Hydrophobic Binding Site Exposed Only on the Intact Receptor. *Biochemistry*, 33, 8991-8997 (1994)
59. Sidenius, N. & Blasi, F.: Domain 1 of the urokinase receptor (uPAR) is required for uPAR-mediated cell binding to vitronectin. *FEBS Letters*, 470, 40-46 (2000)
60. Selleri, C., Montuori, N., Ricci, P., Visconte, V., Carriero, M.V., Sidenius, N., Serio, B., Blasi, F., Rotoli, B., Rossi, G. & Ragno, P.: Involvement of the urokinase-type plasminogen activator receptor in hematopoietic stem cell mobilization. *Blood*, 105, 2198-205 (2005)
61. Resnati, M., Guttinger, M., Valcamonica, S., Sidenius, N., Blasi, F. & Fazioli, F.: Proteolytic cleavage of the urokinase receptor substitutes for the agonist-induced chemotactic effect. *Embo J*, 15, 1572-82 (1996)
62. Resnati, M., Pallavicini, I., Wang, J.M., Oppenheim, J., Serhan, C.N., Romano, M. & Blasi, F.: The fibrinolytic receptor for urokinase activates the G protein-coupled chemotactic receptor FPRL1/LXA4R. *Proc Natl Acad Sci U S A*, 99, 1359-64 (2002)
63. Montuori, N., Visconte, V., Rossi, G. & Ragno, P.: Soluble and cleaved forms of the urokinase-receptor: degradation products or active molecules? *Thromb Haemost.*, 92, 192-8 (2005)
64. Ploug, M. & Ellis, V.: Structure-function relationships in the receptor for urokinase-type plasminogen activator Comparison to other members of the Ly-6 family and snake venom alpha-neurotoxins. *FEBS Letters*, 349, 163-168 (1994)
65. Ploug, M.: Structure-Function Relationships in the Interaction Between the Urokinase- Type Plasminogen Activator and Its Receptor. *Curr Pharm Des.*, 9, 1499-528 (2003)
66. Low, B.W., Preston, H.S., Sato, A., Rosen, L.S., Searl, J.E., Rudko, A.D. & Richardson, J.S.: Three dimensional structure of erabutoxin b neurotoxic protein: inhibitor of acetylcholine receptor. *Proc Natl Acad Sci U S A.*, 73, 2991-4 (1976)
67. Craik, C.S., Sprang, S., Fletterick, R. & Rutter, W.J.: Intron-exon splice junctions map at protein surfaces. *Nature*, 299, 180-2 (1982)
68. Dewan, J.C., Grant, G.A. & Sacchettini, J.C.: Crystal structure of kappa-bungarotoxin at 2.3. Å resolution. *Biochemistry*, 33, 13147-54 (1994)
69. Fletcher, C.M., Harrison, R.A., Lachmann, P.J. & Neuhaus, D.: Structure of a soluble, glycosylated form of the human complement regulatory protein CD59. *Structure*, 2, 185-99 (1994)
70. Pawlak, J., Mackessy, S.P., Fry, B.G., Bhatia, M., Mourier, G., Fruchart-Gaillard, C., Servent, D., Menez, R., Stura, E., Menez, A. & Kini, R.M.: Denmotoxin, a three-finger toxin from the colubrid snake Boiga dendrophila (Mangrove Catsnake) with bird-specific activity. *J Biol Chem*, 281, 29030-41 (2006)
71. Torres, A.M., Kini, R.M., Selvanayagam, N. & Kuchel, P.W.: NMR structure of bucandin, a neurotoxin from the venom of the Malayan krait (Bungarus candidus). *Biochem J*, 360, 539-48 (2001)
72. Petranka, J., Zhao, J., Norris, J., N.B., T., Ware, R.E., Sims, P.J. & Rosse, W.F.: Structure-function relationships of the complement regulatory protein, CD59. *Blood Cells Mol Dis.*, 22, 281-96 (1996)
73. Grant, G.A., Luetje, C.W., Summers, R. & Xu, X.L.: Differential Roles for Disulfide Bonds in the Structural Integrity and Biological Activity of kappa-Bungarotoxin, a Neuronal Nicotinic Acetylcholine Receptor Antagonist. *Biochemistry*, 37, 12166-12171 (1998)
74. Servent, D., Winckler-Dietrich, V., Hu, H.Y., Kessler, P., Drevet, P., Bertrand, D. & Menez, A.: Only snake curaremimetic toxins with a fifth disulfide bond have high affinity for the neuronal alpha7 nicotinic receptor. *J Biol Chem*, 272, 24279-86 (1997)
75. Suh, T., Nerlov, C., Dano, K. & Degen, J.: The murine urokinase-type plasminogen activator receptor gene. *J. Biol. Chem.*, 269, 25992-25998 (1994)
76. Casey, J., Petranka, J., Kottra, J., Fleenor, D. & Rosse, W.: The structure of the urokinase-type plasminogen activator receptor gene. *Blood*, 84, 1151-1156 (1994)
77. Noel, L.S., Champion, B.R., Holley, C.L., Simmons, C.J., Morris, D.C., Payne, J.A., Lean, J.M., Chambers, T.J., Zaman, G., Lanyon, L.E., Suva, L.J. & Miller, L.R.: RoBo-1, a novel member of the urokinase plasminogen activator receptor/CD59/Ly-6/snake toxin family selectively expressed in rat bone and growth plate cartilage. *J Biol Chem*, 273, 3878-83 (1998)
78. Lizano, S., Angulo, Y., Lomonte, B., Fox, J.W., Lambeau, G., Lazdunski, M. & Gutierrez, J.M.: Two phospholipase A2 inhibitors from the plasma of Cerrophidion (Bothrops) godmani which selectively inhibit two different group-II phospholipase A2 myotoxins from its own venom: isolation, molecular cloning and biological properties. *Biochem J*, 346 Pt 3, 631-9 (2000)
79. Okumura, K., Masui, K., Inoue, S., Ikeda, K. & Hayashi, K.: Purification, characterization and cDNA cloning of a phospholipase A2 inhibitor from the serum of the non-venomous snake Elaphe quadrivirgata. *Biochem J*, 341 (Pt 1), 165-71 (1999)
80. Rösel, M., Claas, C., Seiter, S., Herlevsen, M. & Zöller, M.: Cloning and functional characterization of a new phosphatidyl-inositol anchored molecule of a metastasizing rat pancreatic tumor. *Oncogene*, 17, 1989-2002 (1998)
81. Seiter, S., Stassar, M., Rappl, G., Reinhold, U., Tilgen, W. & Zöller, M.: Upregulation of C4.4A Expression During Progression of Melanoma, *J Invest Dermatol* 116, 344-347 (2001)
82. Hansen, L., Lærum, O., Illemann, M., Nielsen, B. & Ploug, M.: Altered expression of the urokinase receptor homologue, C4.4A, in invasive areas of human esophageal squamous cell carcinoma. *Int J Cancer,* 122, 734-41 (2007)

83. Hansen, L.V., Skov, B.G., Ploug, M. & Pappot, H.: Tumour cell expression of C4.4A, a structural homologue of the urokinase receptor, correlates with poor prognosis in non-small cell lung cancer. *Lung Cancer*, 58, 260-6 (2007)
84. Hansen, L.V., Gardsvoll, H., Nielsen, B.S., Lund, L.R., Dano, K., Jensen, O.N. & Ploug, M.: Structural analysis and tissue localization of human C4.4A: a protein homologue of the urokinase receptor. *Biochem. J.*, 380, 845-857 (2004)
85. Klippel, S., Strunck, E., Roder, S., Lubbert, M., Lange, W., Azemar, M., Meinhardt, G., Schaefer, H.-E. & Pahl, H.L.: Cloning of PRV-1, a novel member of the uPAR receptor superfamily, which is overexpressed in polycythemia rubra vera. *Blood*, 95, 2569-2576 (2000)
86. Takayama, T., Mishima, T., Mori, M., Jin, H., Tsukamoto, H., Takahashi, K., Takizawa, T., Kinoshita, K., Suzuki, M., Sato, I., Matsubara, S., Araki, Y. & Takizawa, T.: Sexually Dimorphic Expression of the Novel Germ Cell Antigen TEX101 During Mouse Gonad Development *Biol Reprod*, 72, 1315-1323 (2005)
87. Ploug, M., Ostergaard, S., Gardsvoll, H., Kovalski, K., Holst-Hansen, C., Holm, A., Ossowski, L. & Dano, K.: Peptide-Derived Antagonists of the Urokinase Receptor. Affinity Maturation by Combinatorial Chemistry, Identification of Functional Epitopes, and Inhibitory Effect on Cancer Cell Intravasation. *Biochemistry*, 40, 12157-12168 (2001)
88. Jorgensen, T.J., Gardsvoll, H., Dano, K., Roepstorff, P. & Ploug, M.: Dynamics of urokinase receptor interaction with Peptide antagonists studied by amide hydrogen exchange and mass spectrometry. *Biochemistry*, 43, 15044-57 (2004)
89. Yuan, C. & Huang, M.: Does the urokinase receptor exist in a latent form? *Cellular and Molecular Life Sciences (CMLS)*, 64, 1033-1037 (2007)
90. Ploug, M., Rahbek-Nielsen, H., Ellis, V., Roepstorff, P. & Dano, K.: Chemical Modification of the Urokinase-Type Plasminogen Activator and Its Receptor Using Tetranitromethane. Evidence for the Involvement of Specific Tyrosine Residues in Both Molecules during Receptor-Ligand Interaction. *Biochemistry*, 34, 12524-12534 (1995)
91. Waltz, D. & Chapman, H.: Reversible cellular adhesion to vitronectin linked to urokinase receptor occupancy. *J. Biol. Chem.*, 269, 14746-14750 (1994)
92. Wei, Y., Waltz, D., Rao, N., Drummond, R., Rosenberg, S. & Chapman, H.: Identification of the urokinase receptor as an adhesion receptor for vitronectin. *J. Biol. Chem.*, 269, 32380-32388 (1994)
93. Carriero, M.V., Vecchio, S.D., Capozzoli, M., Franco, P., Fontana, L., Zannetti, A., Botti, G., D'Aiuto, G., Salvatore, M. & Stoppelli, M.P.: Urokinase Receptor Interacts with $alpha_v beta_5$ Vitronectin Receptor, Promoting Urokinase-dependent Cell Migration in Breast Cancer. *Cancer Res*, 59, 5307-5314 (1999)
94. Wei, Y., Eble, J.A., Wang, Z., Kreidberg, J.A. & Chapman, H.A.: Urokinase Receptors Promote $beta_1$ Integrin Function through Interactions with Integrin $alpha_3 beta_1$. *Mol. Biol. Cell*, 12, 2975-2986 (2001)
95. Wei, Y., Lukashev, M., Simon, D.I., Bodary, S.C., Rosenberg, S., Doyle, M.V. & Chapman, H.A.: Regulation of Integrin Function by the Urokinase Receptor *Science*, 273, 1551-1555 (1996)
96. Wei, Y., Czekay, R.P., Robillard, L., Kugler, M.C., Zhang, F., Kim, K.K., Xiong, J.P., Humphries, M.J. & Chapman, H.A.: Regulation of $alpha_5 beta_1$ integrin conformation and function by urokinase receptor binding. *J Cell Biol*, 168, 501-11 (2005)
97. Chaurasia, P., Aguirre-Ghiso, J.A., Liang, O.D., Gardsvoll, H., Ploug, M. & Ossowski, L.: A region in urokinase plasminogen receptor domain III controlling a functional association with $alpha_5 beta_1$ integrin and tumor growth. *J Biol Chem*, 281, 14852-63 (2006)
98. Behrendt, N., Jensen, O.N., Engelholm, L.H., Mortz, E., Mann, M. & Dano, K.: A urokinase receptor-associated protein with specific collagen binding properties. *J Biol Chem*, 275, 1993-2002 (2000)
99. Colman, R.W., Pixley, R.A., Najamunnisa, S., Yan, W., Wang, J., Mazar, A. & McCrae, K.R.: Binding of high molecular weight kininogen to human endothelial cells is mediated via a site within domains 2 and 3 of the urokinase receptor. *J Clin Invest*, 100, 1481-7 (1997)
100. Ploug, M., Laurenborg Hansen, L.B., Holm, A. & Dano, K.: Photoaffinity Labeling of the Human Receptor for Urokinase-Type Plasminogen Activator Using a Decapeptide Antagonist. Evidence for a Composite Ligand-Binding Site and a Short Interdomain Separation. *Biochemistry*, 37, 3612-3622 (1998)
101. Ellis, V.: Functional analysis of the cellular receptor for urokinase in plasminogen activation. Receptor binding has no influence on the zymogenic nature of pro-urokinase. *J Biol Chem*, 271, 14779-84 (1996)
102. Parry, M.A., Zhang, X.C. & Bode, I.: Molecular mechanisms of plasminogen activation: bacterial cofactors provide clues. *Trends Biochem Sci*, 25, 53-9 (2000)
103. Marcotte, P.A., Kozan, I.M., Dorwin, S.A. & Ryan, J.M.: The matrix metalloproteinase pump-1 catalyzes formation of low molecular weight (pro)urokinase in cultures of normal human kidney cells. *J Biol Chem*, 267, 13803-6 (1992)
104. Spraggon, G., Phillips, C., Nowak, U.K., Ponting, C.P., Saunders, D., Dobson, C.M., Stuart, D.I. & Jones, E.Y.: The crystal structure of the catalytic domain of human urokinase-type plasminogen activator. *Structure*, 3, 681-691 (1995)
105. Zhao, G., Yuan, C., Wind, T., Huang, Z., Andreasen, P.A. & Huang, M.: Structural basis of specificity of a peptidyl urokinase inhibitor, upain-1. *J Struct Biol* 160, 1-10 (2007)
106. Rockway, T.W. & Giranda, V.L.: Inhibitors of the proteolytic activity of urokinase type plasminogen activator. *Curr Pharm Des*, 9, 1483-98 (2003)
107. Appella, E., Robinson, E., Ullrich, S., Stoppelli, M., Corti, A., Cassani, G. & Blasi, F.: The receptor-binding sequence of urokinase. A biological function for the growth-factor module of proteases. *J. Biol. Chem.*, 262, 4437-4440 (1987)
108. Magdolen, V., Rettenberger, P., Koppitz, M., Goretzki, L., Kessler, H., Weidle, U.H., König, B., Graeff, H., Schmitt, M. & Wilhelm, O.: Systematic mutational analysis of the receptor-binding region of the human urokinase-type plasminogen activator. *Eur J Biochem*, 237, 743-51 (1996)

109. Burgle, M., Koppitz, M., Riemer, C., Kessler, H., König, B., Weidle, U.H., Kellermann, J., Lottspeich, F., Graeff, H., Schmitt, M., Goretzki, L., Reuning, U., Wilhelm, O. & Magdolen, V.: Inhibition of the interaction of urokinase-type plasminogen activator (uPA) with its receptor (uPAR) by synthetic peptides. *Biol Chem*, 378, 231-7 (1997)
110. Schmiedeberg, N., Schmitt, M., Rolz, C., Truffault, V., Sukopp, M., Burgle, M., Wilhelm, O.G., Schmalix, W., Magdolen, V. & Kessler, H.: Synthesis, solution structure, and biological evaluation of urokinase type plasminogen activator (uPA)-derived receptor binding domain mimetics. *J Med Chem*, 45, 4984-94 (2002)
111. Hansen, A.P., Petros, A.M., Meadows, R.P., Nettesheim, D.G., Mazar, A.P., Olejniczak, E.T., Xu, R.X., Pederson, T.M., Henkin, J. & Fesik, S.W.: Solution Structure of the Amino-Terminal Fragment of Urokinase-Type Plasminogen Activator. *Biochemistry*, 33, 4847-4864 (1994)
112. Nowak, U.K., Li, X., Teuten, A.J., Smith, R.A.G. & Dobson, C.M.: NMR studies of the dynamics of the multidomain protein urokinase-type plasminogen activator. *Biochemistry*, 32, 298-309 (1993)
113. Oswald, R.E., Bogusky, M.J., Bamberger, M., Smith, R.A.G. & Dobson, C.M.: Dynamics of the multidomain fibrinolytic protein urokinase from two-dimensional NMR, *Nature* 337, 579-582 (1989)
114. Novokhatny, V., Medved, L., Mazar, A., Marcotte, P., Henkin, J. & Ingham, K.: Domain structure and interactions of recombinant urokinase-type plasminogen activator. *J. Biol. Chem.*, 267, 3878-3885 (1992)
115. Hansen, A.P., Petros, A.M., Meadows, R.P. & Fesik, S.W.: Backbone Dynamics of a Two-Domain Protein: 15N Relaxation Studies of the Amino-Terminal Fragment of Urokinase-Type Plasminogen Activator. *Biochemistry*, 33, 15418-15424 (1994)
116. Huang, M., Mazar, A.P., Parry, G., Higazi, A.A.-R., Kuo, A. & Cines, D.B.: Crystallization of soluble urokinase receptor (suPAR) in complex with urokinase amino-terminal fragment (1-143)
Acta Crystallographica Section D, 61, 697-700 (2005)
117. Gardsvoll, H., Gilquin, B., Le Du, M.H., Menéz, A., Jorgensen, T.J.D. & Ploug, M.: Characterization of the Functional Epitope on the Urokinase Receptor: Complete Alanine Scanning Mutagenesis Supplemented by Chemical Cross-linking *J. Biol. Chem.*, 281, 19260-19272 (2006)
118. Bdeir, K., Kuo, A., Sachais, B.S., Rux, A.H., Bdeir, Y., Mazar, A., Higazi, A.A. & Cines, D.B.: The kringle stabilizes urokinase binding to the urokinase receptor. *Blood*, 102, 3600-8 (2003)
119. Waltz, D.A., Sailor, L.Z. & Chapman, H.A.: Cytokines induce urokinase-dependent adhesion of human myeloid cells. A regulatory role for plasminogen activator inhibitors. *J Clin Invest.*, 91, 1541-52 (1993)
120. Chang, A.W., Kuo, A., Barnathan, E.S. & Okada, S.S.: Urokinase receptor-dependent upregulation of smooth muscle cell adhesion to vitronectin by urokinase. *Arterioscler Thromb Vasc Biol*, 18, 1855-60 (1998)
121. Kanse, S.M., Kost, C., Wilhelm, O.G., Andreasen, P.A. & Preissner, K.T.: The urokinase receptor is a major vitronectin-binding protein on endothelial cells. *Exp Cell Res*, 224, 344-53 (1996)
122. Gardsvoll, H. & Ploug, M.: Mapping of the vitronectin binding site on the urokinase receptor. Involvement of a coherent receptor interface comprising residues from both domain I and the flanking interdomain linker region *J. Biol. Chem.*, 282, 13561-13572 (2007)
123. Sidenius, N., Andolfo, A., Fesce, R. & Blasi, F.: Urokinase Regulates Vitronectin Binding by Controlling Urokinase Receptor Oligomerization. *J. Biol. Chem.*, 277, 27982-27990 (2002)
124. Kjoller, L.: The urokinase plasminogen activator receptor in the regulation of the actin cytoskeleton and cell motility. *Biol Chem.*, 383, 5-19 (2002)
125. Madsen, C.D., Ferraris, G.M., Andolfo, A., Cunningham, O. & Sidenius, N.: uPAR-induced cell adhesion and migration: vitronectin provides the key. *J Cell Biol*, 177, 927-39 (2007)
126. Salasznyk, R.M., Zappala, M., Zheng, M., Yu, L., Wilkins-Port, C. & McKeown-Longo, P.J.: The uPA receptor and the somatomedin B region of vitronectin direct the localization of uPA to focal adhesions in microvessel endothelial cells. *Matrix Biol*, 26, 359-70 (2007)
127. Preissner, K.T. & Seiffert, D.: Role of vitronectin and its receptors in haemostasis and vascular remodeling. *Thromb Res*, 89, 1-21 (1998)
128. Lynn, G.W., Heller, W.T., Mayasundari, A., Minor, K.H. & Peterson, C.B.: A model for the three-dimensional structure of human plasma vitronectin from small-angle scattering measurements. *Biochemistry*, 44, 565-74 (2005)
129. Horn, N.A., Hurst, G.B., Mayasundari, A., Whittemore, N.A., Serpersu, E.H. & Peterson, C.B.: Assignment of the Four Disulfides in the N-terminal Somatomedin B Domain of Native Vitronectin Isolated from Human Plasma. *J. Biol. Chem.*, 279, 35867-35878 (2004)
130. Kamikubo, Y., Kroon, G., Curriden, S.A., Dyson, H.J. & Loskutoff, D.J.: The Reduced, Denatured Somatomedin B Domain of Vitronectin Refolds into a Stable, Biologically Active Molecule. *Biochemistry*, 45, 3297-3306 (2006)
131. Kamikubo, Y.-i., Okumura, Y. & Loskutoff, D.J.: Identification of the Disulfide Bonds in the Recombinant Somatomedin B Domain of Human Vitronectin. *J. Biol. Chem.*, 277, 27109-27119 (2002)
132. Li, X., Zou, G., Yuan, W. & Lu, W.: Defining the Native Disulfide Topology in the Somatomedin B Domain of Human Vitronectin *J. Biol. Chem.*, 282, 5318-5326 (2007)
133. Zhou, A.: Functional structure of the somatomedin B domain of vitronectin. *Protein Sci*, 16, 1502-8 (2007)
134. Kamikubo, Y., DeGuzman, R., Kroon, G., Curriden, S., Neels, J.G., Churchill, M.J., Dawson, P., Oldziej, S., Jagielska, A., Scheraga, H.A., Loskutoff, D.J. & Dyson, H.J.: Disulfide Bonding Arrangements in Active Forms of the Somatomedin B Domain of Human Vitronectin. *Biochemistry*, 43, 6519-6534 (2004)
135. Kjaergaard, M., Gardsvoll, H., Hirschberg, D., Nielbo, S., Mayasundari, A., Peterson, C.B., Jansson, A., Jorgensen, T.J., Poulsen, F.M. & Ploug, M.: Solution structure of recombinant somatomedin B domain from vitronectin produced in Pichia pastoris. *Protein Sci*, 16, 1934-45 (2007)

136. Mayasundari, A., Whittemore, N.A., Serpersu, E.H. & Peterson, C.B.: The Solution Structure of the N-terminal Domain of Human Vitronectin: Proximal Sites That Regulate Fibrinolysis and Cell Migration. *J. Biol. Chem.*, 279, 29359-29366 (2004)
137. Zhou, A., Huntington, J.A., Pannu, N.S., Carrell, R.W. & Read, R.J.: How vitronectin binds PAI-1 to modulate fibrinolysis and cell migration. *Nat Struct Biol.*, 10, 541-544 (2003)
138. Deng, G., Curriden, S., Wang, S., Rosenberg, S. & Loskutoff, D.: Is plasminogen activator inhibitor-1 the molecular switch that governs urokinase receptor-mediated cell adhesion and release?
. *J. Cell Biol.*, 134, 1563-1571 (1996)
139. Waltz, D.A., Natkin, L.R., Fujita, R.M., Wei, Y. & Chapman, H.A.: Plasmin and plasminogen activator inhibitor type 1 promote cellular motility by regulating the interaction between the urokinase receptor and vitronectin. *J Clin Invest*, 100, 58-67 (1997)
140. Stefansson, S. & Lawrence, D.A.: The serpin PAI-1 inhibits cell migration by blocking integrin a_Vb_3 binding to vitronectin. *Nature*, 383, 441-3 (1996)
141. Okumura, Y., Kamikubo, Y., Curriden, S.A., Wang, J., Kiwada, T., Futaki, S., Kitagawa, K. & Loskutoff, D.J.: Kinetic Analysis of the Interaction between Vitronectin and the Urokinase Receptor
J. Biol. Chem., 277, 9395-9404 (2002)
142. Moser, T.L., Enghild, J.J., Pizzo, S.V. & Stack, M.S.: Specific binding of urinary-type plasminogen activator (u-PA) to vitronectin and its role in mediating u-PA-dependent adhesion of U937 cells. *Biochem J.*, 307, 867-73 (1995)

Footnote:
http://www.ncbi.nlm.nih.gov/Structure/cdd/cddsrv.cgi?uid=smart00134

Abbreviations: ATF, amino terminal fragment; ANS, 8-anilino-1-naphthalene sulfonate; GFD, growth factor-like domain; GPI, glycosylphosphatidylinositol; PNH, paroxysmal nocturnal haemoglobinuria; SMB, somatomedin B domain of vitronectin; uPA, urokinase-type plasminogen activator; uPAR, uPA receptor

Key Words: LU-domain, CD87, GPI, multidomain, cancer, three-finger fold, *alpha*-neurotoxin, ANS, vitronectin, uPA, LYPD, PLAUR, gene cluster, SMB, TEX 101, C4.4A, PRV-1, PRO4356, GPQH2552, Review

Send correspondence to: Michael Ploug, Ph.D., D.Sc., Finsen Laboratory, Rigshospitalet section 3735, Copenhagen Biocenter room 3.3.31., Ole Maaloes Vej 5, DK-2200 Copenhagen N, Denmark. Tel: 45-35456037, Fax: 45-35453797, E-mail: m-ploug@finsenlab.dk